

An auditory-periphery model of the effects of acoustic trauma on auditory nerve responses

Ian C. Bruce,^{a)} Murray B. Sachs, and Eric D. Young

Center for Hearing Sciences and Department of Biomedical Engineering, Johns Hopkins University
School of Medicine, Baltimore, Maryland 21205

(Received 20 June 2002; revised 12 September 2002; accepted 16 September 2002)

Acoustic trauma degrades the auditory nerve's tonotopic representation of acoustic stimuli. Recent physiological studies have quantified the degradation in responses to the vowel /ε/ and have investigated amplification schemes designed to restore a more correct tonotopic representation than is achieved with conventional hearing aids. However, it is difficult from the data to quantify how much different aspects of the cochlear pathology contribute to the impaired responses. Furthermore, extensive experimental testing of potential hearing aids is infeasible. Here, both of these concerns are addressed by developing models of the normal and impaired auditory peripheries that are tested against a wide range of physiological data. The effects of both outer and inner hair cell status on model predictions of the vowel data were investigated. The modeling results indicate that impairment of both outer and inner hair cells contribute to degradation in the tonotopic representation of the formant frequencies in the auditory nerve. Additionally, the model is able to predict the effects of frequency-shaping amplification on auditory nerve responses, indicating the model's potential suitability for more rapid development and testing of hearing aid schemes.
© 2003 Acoustical Society of America. [DOI: 10.1121/1.1519544]

PACS numbers: 43.64.Bt, 43.64.Pg, 43.64.Sj, 43.66.Ts [BLM]

I. INTRODUCTION

Recent physiological studies (Miller *et al.*, 1997; Schilling *et al.*, 1998; Wong *et al.*, 1998; Miller *et al.*, 1999a, b) have shown that acoustic trauma causes substantial changes in the auditory nerve (AN) representation of a speechlike stimulus, in this case the synthesized vowel /ε/ as in "met." The responses of a normal AN fiber to the vowel presented at stimulus levels appropriate for conversational speech are dominated by the formant frequency nearest the fiber's best frequency (BF), a phenomenon known as synchrony capture (Young and Sachs, 1979; Deng and Geisler, 1987b; Deng *et al.*, 1987; Miller *et al.*, 1997). In contrast, fibers in an ear impaired by acoustic trauma respond to a broad range of frequency components in the vowel, particularly to formants at frequencies below the fibers' BFs. As a result, the normal tonotopic representation of the vowel is degraded; most important, responses to the first formant ($F1$) spread away from their tonotopically appropriate location towards higher BFs. The upward spread of $F1$ responses means that cochlear locations at which responses to $F2$ and $F3$ are normally seen now respond primarily to $F1$. This spread of $F1$ response reduces the quality of the representation of $F2$ and $F3$; for example, the discriminability, based on AN responses, of vowels with different $F2$ s is substantially reduced (Miller *et al.*, 1999b). In this paper, we describe a computational model of the auditory periphery that is able to describe this degradation of AN representation of speech stimuli.

Anatomical investigations of acoustically traumatized

cochleae show damage to both the outer (OHC) and inner (IHC) hair cells (Liberman and Dodds, 1984a). OHC impairment produces broadened and elevated AN fiber threshold tuning curves (e.g., Kiang *et al.*, 1976; Robertson, 1982; Liberman and Dodds, 1984a). Also observed are reductions in nonlinearities in AN responses, such as two-tone rate suppression (Schmiedt *et al.*, 1980, 1990; Salvi *et al.*, 1982; Miller *et al.*, 1997) and the compressive nature of basilar-membrane (BM) responses (Robles and Ruggero, 2001). The latter are seen, for example, in the growth of discharge rate of AN fibers with sound level (Harrison, 1981). IHC damage causes elevation of AN fiber threshold tuning curves without broadening their tuning (Liberman and Dodds, 1984a).

Because the cochlea is nonlinear, it is difficult to attribute changes in AN responses to speech following acoustic trauma to particular aspects of the damage, such as IHC versus OHC or tuning versus compression. A model is helpful in that process. The effects of broadened tuning on responses to speech have been studied using computational models (Geisler, 1989; Sachs *et al.*, 2002), but these models do not include two-tone rate suppression (the former also lacks BM compression), and IHC impairment was not investigated. Our methodology in this paper is to modify the OHC and IHC sections of an auditory periphery model (Zhang *et al.*, 2001) to produce the desired impairment of model AN fiber tuning curves, both threshold and bandwidth, and observe the effects of these changes on model responses to the vowel. The physiological accuracy of the model's predictions is assessed by comparison with published data. This sort of model should be useful as a means of quickly and efficiently testing potential hearing-aid amplification schemes and will provide a kind of test not commonly used, which is to evaluate the ability of amplification to restore normal patterns of auditory nerve activity in response to speech. Such informa-

^{a)}Author to whom correspondence should be addressed. Department of Electrical and Computer Engineering, Room CRL-229, McMaster University, 1280 Main Street West, Hamilton, Ontario L8S 4K1, Canada. Electronic mail: ibruce@ieee.org

tion should be a useful adjunct to psychophysical testing.

We have selected the model of Zhang *et al.* (2001) because it has a number of features that make it suitable to the task. First, the model input can be any arbitrary sound-pressure waveform and its output consists of simulated AN fiber spike times, so the same types of data analyses can be performed on the model as on the physiological data. Second, the model has been designed particularly to describe the synchrony (or phase locking) behavior of low-frequency AN fibers. Synchronized response are important to this effort because synchrony shows directly to which frequency components of a complex stimulus a fiber is responding. Synchrony is particularly revealing when used to analyze the effects of impairment on responses to speech. Third, the model contains sections that separately represent the IHCs and OHCs, making it possible to simulate effects of damage to particular aspects of cochlear function. Fourth, the model parameters have been adjusted for the cat auditory periphery and the model has been extensively validated by comparison with data from cat, the same species in which the comparison vowel data were collected.

There exist a number of alternative models of the auditory periphery, which we decided were less suitable to the task at hand. The model of Zhang *et al.* (2001) is based on an earlier model by Carney (1993). The latter model accounts for variation of frequency tuning with stimulus level and BM compression but does not produce two-tone rate suppression, which has been shown to be important in AN responses to speech (Young and Sachs, 1979; Sachs and Young, 1979; Miller *et al.*, 1997; Wong *et al.*, 1998). Models by Deng and Geisler (1987a), Payton (1988), Jenison *et al.* (1991), and Giguère and Woodland (1994) also do not include two-tone rate suppression and have not been as extensively validated against physiological data. The models of Kates (1995) and Robert and Eriksson (1999) do include two-tone rate suppression, but this is achieved via feedback control from neighboring BM filters. Such lateral feedback does not have an obvious correlate in cochlear physiology and could lead to unpredictable effects when one section is impaired but adjacent sections are normal. Several studies have modeled the nonlinear properties of the BM, including level-dependent tuning, compression, and two-tone rate suppression (Pfeiffer, 1970; Duifhuis, 1976; Goldstein, 1990, 1995; Meddis *et al.*, 2001; Irino and Patterson, 2001; Lopez-Poveda and Meddis, 2001). The more recent of these models produce some features not seen in the Zhang *et al.* (2001) model, such as a shift in BF with intensity (as reported by Anderson *et al.*, 1971; Johnstone *et al.*, 1986; Zhang and Zwislocki, 1996; Robles and Ruggero, 2001) and abrupt phase changes in AN responses at very high stimulus levels (the component 1/component 2 transition, Liberman and Kiang, 1984). However, these BM models do not include IHCs, synapses, and AN fibers and therefore are not suitable for comparison with AN data (Meddis *et al.*, 2001).

Although the Zhang *et al.* (2001) model is accurate in predicting a large range of physiological data for pure-tone and two-tone stimuli, it has not been tested previously with speechlike stimuli. In this paper, we show that some changes to the OHC control of BM tuning are required to improve the

model's predictions of normal AN responses to the vowel stimulus. A simple modification of OHC function in our improved model allows the effects of acoustic trauma to be modeled, including various degrees of elevation and broadening of tuning curves and a proportional loss of compression and suppression. An analogous modification to the IHC section of the model leads primarily to elevation of the tuning curve without substantially changing the bandwidth as measured by Q_{10} values. These different effects of OHC and IHC impairment are consistent with the physiological data (e.g., Liberman and Dodds, 1984a). Here we show that both IHC and OHC impairment can cause model fibers with BFs near the second and third formants to lose synchrony to those formants and become more synchronized to other components of the vowel spectrum, as observed in the physiological data. The model also predicts that the amplification scheme previously suggested by Miller *et al.* (1999a) restores synchrony capture by the second formant for model fibers with BFs in the second formant region.

II. MODELING THE NORMAL AUDITORY PERIPHERY

The auditory-periphery model, modified from Zhang *et al.* (2001), comprises several sections, each providing a phenomenological description of a different part of cochlear function. The model is illustrated in the schematic diagram of Fig. 1(a). The details of the normal model can be found in Zhang *et al.* (2001). In this paper we only describe modifications made to the Zhang *et al.* model to improve its accuracy in predicting responses to speech sounds and the changes that are needed to model OHC and IHC impairment. The model code is available on request. All the changes to the normal AN-periphery model from that of Zhang *et al.* (2001) are summarized in Table I.

The first section models the filtering properties of the middle ear (ME), described in detail in Appendix A. Filtering by the outer ear is not included, because we are using the model to predict physiological data for acoustic stimuli that were delivered directly to the tympanic membrane via earbars (e.g., Miller *et al.*, 1997). Outer-ear filtering would need to be considered for free-field acoustic stimulation.

The second section describes the "control path," which includes a wideband, nonlinear, time-varying, band-pass filter followed by an OHC nonlinearity (NL) and low-pass (LP) filter. The purpose of this section is to control the time-varying, nonlinear behavior of the narrow-band signal-path BM filter, which it does by adjusting the bandwidth and gain of that filter through its time constant τ_{sp} . The control-path filter must be wider than the signal-path filter to account for wideband nonlinear phenomena such as two-tone rate suppression (e.g., Sachs and Kiang, 1968; Costalupes *et al.*, 1987; Javel *et al.*, 1978, 1983; Delgutte, 1990; Temchin *et al.*, 1997).

The third section of the model is the "signal path" describing the filter properties and traveling wave delay of the BM (time-varying, narrow-band filter); the nonlinear transduction and low-pass filtering of the IHC (IHC NL and LP); spontaneous and driven activity and adaptation in synaptic transmission (synapse model); and spike generation and refractoriness in the AN (spike generator). The center fre-

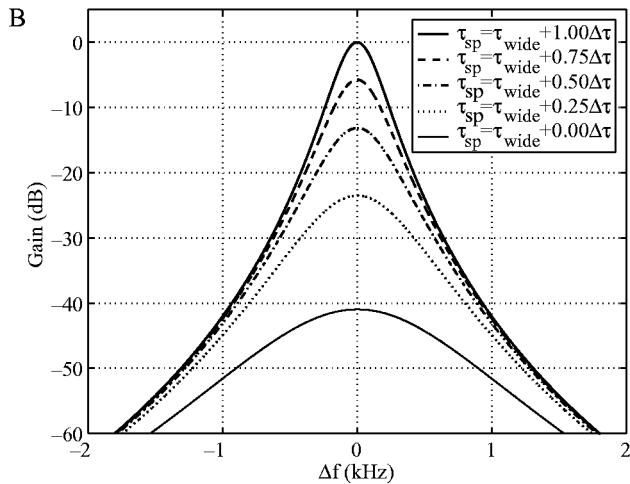
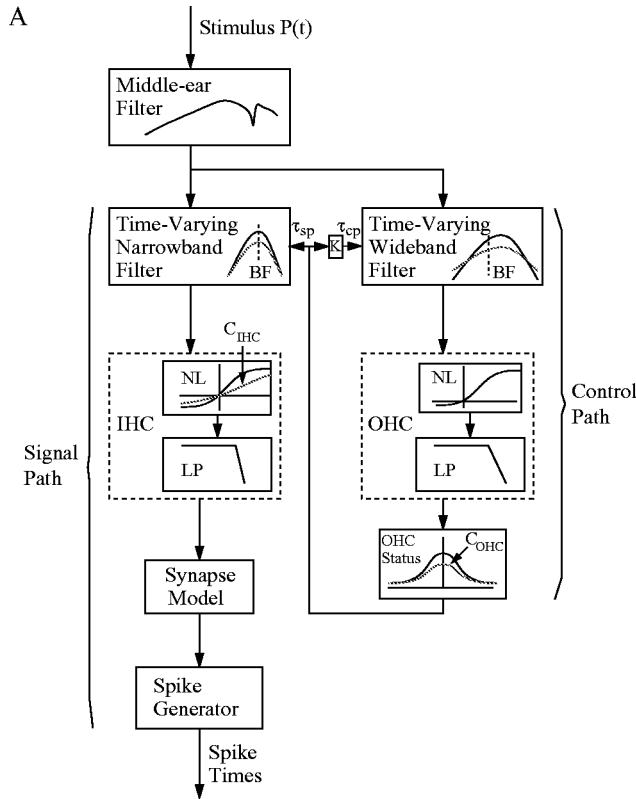


FIG. 1. (a) The auditory-periphery model modified from Zhang *et al.* (2001) (cf. Fig. 1 of that paper). Abbreviations: outer hair cell (OHC); low-pass (LP) filter; static nonlinearity (NL); inner hair cell (IHC); best frequency (BF). C_{IHC} and C_{OHC} are scaling constants that control IHC and OHC status, respectively. (b) Gain functions of linear versions of the time-varying narrow-band filter in the signal path, plotted as gain versus frequency deviation Δf from BF. The filter is fourth-order and is plotted for five different values of τ_{sp} between τ_{narrow} and τ_{wide} ; $\Delta\tau = \tau_{narrow} - \tau_{wide}$. τ_{narrow} was chosen to produce a 10-dB bandwidth of ~ 450 Hz, and τ_{wide} was chosen to produce a maximum gain change at BF of ~ 41 dB. This plot can be interpreted as showing the nominal tuning of the filter with normal OHC function at five different sound pressure levels or alternatively as the nominal tuning of the filter for five different degrees of OHC impairment.

quency of the signal-path BM filter is the primary determinant of the model fiber's BF. The bandwidth and gain of both the signal-path, narrow-band filter and the control-path, wideband filter are varied continuously as a function of the control path output. The low-pass filtering of the IHC de-

TABLE I. Summary of differences between the normal auditory periphery models of Zhang *et al.* (2001) and of this paper.

Zhang <i>et al.</i> (2001)	This paper
No middle-ear filtering	Middle-ear filtering as described in Appendix A
Synapse gain compensates for IHC filtering	Synapse gain compensates for IHC and ME filtering [see Eq. (1)]
Symmetric nonlinearity between wideband filter and OHC Boltzmann nonlinearity	Linear scaling of 4×10^3 after wideband filter to compensate for removal of symmetric nonlinearity
Wideband-filter gain normalized to unity at BF	Wideband-filter gain normalized to match narrow-band-filter gain at BF (see Appendix B)
OHC LP filter cutoff=800 Hz	OHC LP filter cutoff=600 Hz
BM gain versus BF based on other species	BM gain versus BF estimated from cat AN data [see Eq. (B3)]

scribes the fall-off in pure-tone synchrony with increasing BF above 1 kHz. The preceding IHC nonlinearity produces a dc component in the IHCs of high-BF model fibers, providing nonsynchronized synaptic drive to such fibers. The spontaneous rate (in this paper, 50 spikes/second before the effects of refractoriness), adaptation properties, and rate-level behavior (including threshold and saturation) of a model fiber are determined by the synapse model. Only high spontaneous rate fibers are modeled. The spiking and refractory behavior are set to model the statistics of spike timing in AN fibers.

A. Middle-ear filter

A ME filter was not included in the Zhang *et al.* (2001) model but is important in modeling responses to wideband stimuli such as vowels, because the ME filter changes the relative levels of stimulus components. We have added a ME section to the model by combining the ME-cavities model of Peake *et al.* (1992) with the ME (with cavities open) model of Matthews (1983). A digital-filter representation of this model is described in Appendix A. The ME model has a maximum gain of 32 dB [Fig. 19(b)]. Because the parameters of the Zhang *et al.* (2001) model are set for no ME model, we scale the gain of the ME filter to a maximum gain of 0 dB. This allows us to avoid adjusting other level-dependent parameters of the auditory periphery model. The principal effect of the ME filter is on model thresholds, which are shown by the black dashed line in Fig. 2(a) and are compared to experimental data (Miller *et al.*, 1997).

There are three differences between model and data. First, the model thresholds are consistently higher than experimental ones, which requires an increase in the synapse gain (see below) relative to that of Zhang *et al.* (2001). Second, the model does not accurately reproduce the slope of the best threshold curve below 1 kHz [BTC; thin dashed line in Fig. 2(a)]. Low-frequency thresholds in cat preparations vary from animal to animal (e.g., Liberman, 1978) and are affected by the status of the middle ear bulla cavity (open or

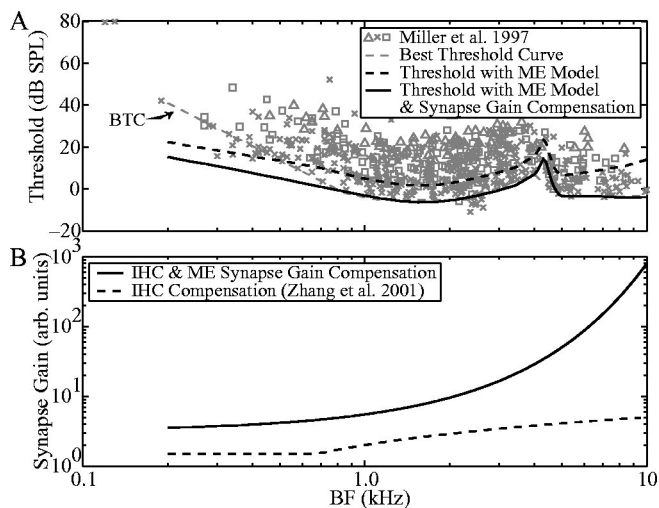


FIG. 2. (a) Thresholds versus BF. The gray symbols are single-fiber thresholds and the thin dashed line is the best threshold curve (BTC) for these data (Miller *et al.*, 1997). The black dashed line shows the model threshold with the ME included. The black solid line shows the model threshold with the ME included plus frequency compensation in the synapse gain for the low-pass filtering of the ME (at ~ 4.5 kHz), as described below. (b) Synapse gain [parameter K_{CF} in Eq. (A17) of Zhang *et al.*, 2001] as a function of BF. The dashed line shows the function used in Zhang *et al.* (2001), which compensates for the low-pass filtering of the IHC to create constant thresholds as a function of BF without ME filtering. The solid line shows the new function described by Eq. (1) that also compensates for the low-pass filtering of the ME to create constant thresholds above ~ 1 kHz, except for the notch just above 4 kHz [see panel (a)].

closed; Guinan and Peake, 1967). The model gives thresholds near the lower end of the published range and the particular data shown are near the upper end. In order to better fit the thresholds at low frequencies, the ME gain function or the synapse gain could be changed. Neither has been done here, because of the uncertainty in the data. Third, the low-pass filtering of the ME produces elevated thresholds for BFs above 4.5 kHz relative to thresholds in the BF region around 1.5 kHz. In contrast, thresholds in the experimental data are similar in these two regions. In Zhang *et al.* (2001) the synapse gain (i.e., the function relating the IHC potential to the synaptic release rate) varied as a function of BF to compensate for the low-pass filtering of the IHC, thus maintaining a constant AN-fiber threshold as a function of BF. We propose that the synapse gain also compensates for the low-pass filtering of the ME above 4.5 kHz. This can be achieved in the model by using a new function for the synapse gain [parameter K_{CF} in Eq. (A17) of Zhang *et al.*, 2001]:

$$K_{CF} = 10^{0.24BF + 0.5}, \quad (1)$$

where BF has the units of kHz. This new function also includes an increase in the absolute gain so that model thresholds better match the BTC. Plotted in Fig. 2(b) are the old (dashed line) and new (solid line) functions.

B. OHC control of BM tuning

The signal-path BM filters are fourth-order, nonlinear, infinite impulse response (IIR) gamma-tone filters (Patterson *et al.*, 1988). Each filter is realized by cascading three nonlinear and one linear first-order, low-pass filters (Zhang *et al.*, 2001). The stimulus waveform is first down-shifted in

frequency by the desired center frequency of the filter, then filtered, and finally up-shifted to its original frequencies. Each of the three nonlinear low-pass filters may be described by the difference equation [modified from Eq. (A4) of Carney (1993)]:

$$y[n] = c1_{LP}[n]y[n-1] + c2_{LP}[n](x[n] + x[n-1]), \quad (2)$$

where x is the filter input, y is the filter output, n is the sample number, and the filter coefficients $c1_{LP}[n]$ and $c2_{LP}[n]$ are determined by the time constant for the signal-path filter $\tau_{sp}[n]$ [see Fig. 1(a)] according to the bilinear transform (Oppenheim and Schaffer, 1989):

$$c1_{LP}[n] = (\tau_{sp}[n]2F_s - 1) / (\tau_{sp}[n]2F_s + 1) \quad (3)$$

and

$$c2_{LP}[n] = 1 / (\tau_{sp}[n]2F_s + 1), \quad (4)$$

where the sampling frequency F_s is set at 500 kHz (Zhang *et al.*, 2001). The time constant $\tau_{sp}[n]$ determines both the gain and the bandwidth of the filter and varies between the values τ_{narrow} and τ_{wide} according to the output signal of the control path. Note that the control path is modified somewhat from that of Zhang *et al.* (2001) to improve the filter dynamics—see Appendix B for details. The single linear LP filter that follows the three nonlinear LP filters in the signal-path BM filters is identical to the nonlinear filters except that its time constant is always τ_{wide} and its dc gain (i.e., the gain at BF) is always unity. Figure 1(b) shows the gain of the signal-path filter for values of τ_{sp} over its whole range; decreasing τ_{sp} from τ_{narrow} to τ_{wide} increases both the bandwidth and the attenuation.

We will consider the behavior of the nonlinear signal-path filter over three different ranges of stimulus intensity. First, at low stimulus intensities the control path signal is negligible and therefore $\tau_{sp}[n] \approx \tau_{narrow}$. Consequently, the bandwidth is narrow, gain is high, and the filter is effectively linear. Second, at moderate stimulus intensities the control path signal becomes significant, such that $\tau_{sp}[n]$ dynamically varies between τ_{narrow} and τ_{wide} , creating effectively broadened tuning, a compressive nonlinearity for stimuli with frequency components near BF, and two-tone suppression for wideband stimuli. The time constant of the control-path filter $\tau_{cp}[n]$ is set to a constant fraction K of $\tau_{sp}[n]$, to create an area of suppression that is appropriately wider than the excitation tuning curve (Zhang *et al.*, 2001). Two-tone rate suppression is created in the model when a suppressor tone produces negligible energy at the output of the signal-path filter but has enough energy at the output of the broader control-path filter to reduce $\tau_{sp}[n]$ via the control path and consequently reduce the gain of the signal-path filter. Third, for very large signals, the control path saturates and $\tau_{sp}[n]$ has an essentially constant value near τ_{wide} . Thus, at high intensities the filter has a broad bandwidth and low gain and is once more linear. These properties simulate the BM tuning and nonlinearities that are caused by the activity of healthy OHCs (e.g., Johnstone *et al.*, 1986; Robles and Ruggero, 2001).

The value of the time constant τ_{narrow} determines the bandwidth of model threshold tuning curves. The bandwidth

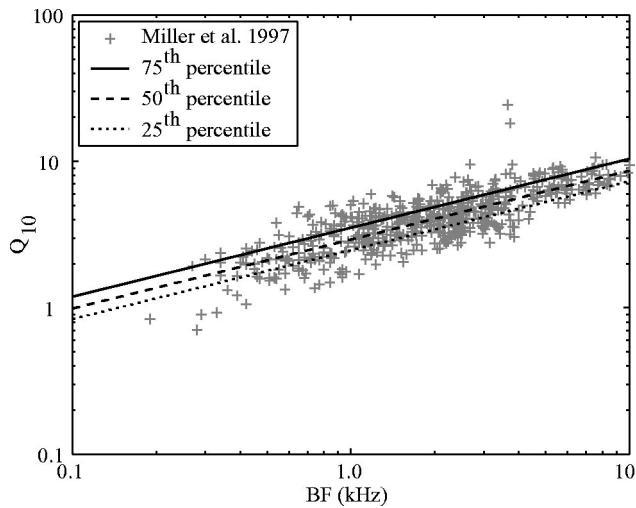


FIG. 3. Normal-cat Q_{10} values as a function of BF from Miller *et al.* (1997). The gray symbols indicate values for individual fibers and lines indicate the 75th (solid line), 50th (dashed line), and 25th (dotted line) percentiles of Q_{10} values after normalization by a linear fit of $\log(Q_{10})$ versus $\log(\text{BF})$.

of a tuning curve is usually quantified according to its Q_{10} value, which is equal to BF divided by the bandwidth of the tuning curve 10 dB above threshold at BF. The desired Q_{10} value can be produced in the model by setting $\tau_{\text{narrows}} = 2Q_{10}/(2\pi\text{BF})$ [Eq. (4) of Zhang *et al.*, 2001]. In Secs. IV A, IV B, and IV D, where data from individual AN fibers are presented, we match model Q_{10} values to the example fibers. In Sec. IV C, where data from populations of AN fibers are presented, we use functional relationships to describe trends in Q_{10} versus BF observed in the population data. In Fig. 3, Q_{10} values from the normal-cat data of Miller *et al.* (1997) are plotted as gray symbols as a function of BF on a log-log scale. Zhang *et al.* (2001) used a linear fit of $\log(Q_{10})$ values from these data versus $\log(\text{BF})$ to set model Q_{10} values. However, at any particular BF there is a range of Q_{10} values observed in the data. AN fibers with different Q_{10} values are likely to have somewhat different responses to wideband stimuli such as vowels. Therefore, in this paper we use the three different functions for Q_{10} versus BF shown in Fig. 3, which correspond to the 75th, 50th, and 25th percentiles of Q_{10} values after normalization by the linear fit of $\log(Q_{10})$ versus $\log(\text{BF})$. The equations for the these functions are, respectively,

$$\log_{10} Q_{10}^{75\text{th}} = 0.4708 \log_{10}(\text{BF}) + 0.5469, \quad (5)$$

$$\log_{10} Q_{10}^{50\text{th}} = 0.4708 \log_{10}(\text{BF}) + 0.4664, \quad (6)$$

$$\log_{10} Q_{10}^{25\text{th}} = 0.4708 \log_{10}(\text{BF}) + 0.3934, \quad (7)$$

where BF has the units of kHz.

The value of the time constant τ_{wide} determines the maximum bandwidth and the minimum gain of the signal-path narrow-band filter, as illustrated in Fig. 1(b). Zhang *et al.* (2001) refer to the difference in filter gain between τ_{narrow} and τ_{wide} as the cochlear amplifier (CA) gain. Based on the third-order nonlinear filter, $\tau_{\text{wide}} = \tau_{\text{narrow}} 10^{-\text{gain}_{\text{CA}}(\text{BF})/60}$, where $\text{gain}_{\text{CA}}(\text{BF})$ is determined by

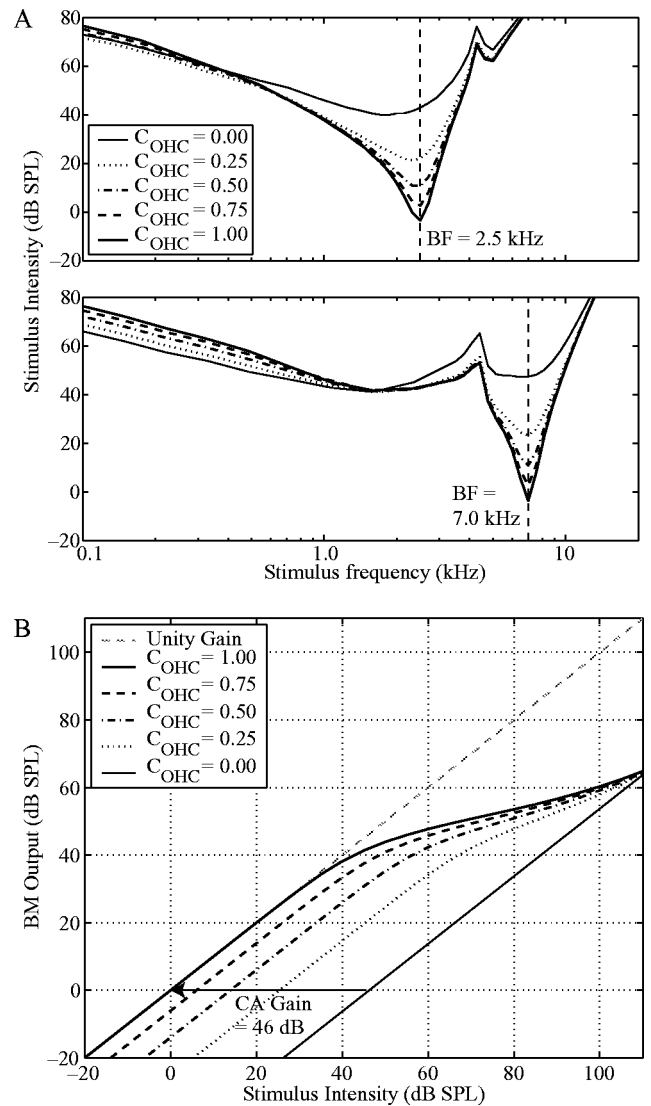


FIG. 4. (a) Model tuning curves as a function of OHC impairment: no impairment $\Rightarrow C_{\text{OHC}} = 1.00$; complete impairment $\Rightarrow C_{\text{OHC}} = 0.00$. Top panel: BF = 2.5 kHz; Bottom panel: BF = 7.0 kHz. (b) The effects of C_{OHC} on BM compression for a fiber with BF = 2.5 kHz. The thin dashed line shows a linear input/output function (no compression), shallower slopes indicate compression. The arrow indicates that normal OHC function produces a difference in the filter gain of 46 dB between low-intensity stimuli and high-intensity stimuli at a BF of 2.5 kHz. At moderate intensities the filter is normally compressive, i.e., slope < 1 . This cochlear amplifier (CA) gain and associated compression are progressively lost with increasing OHC impairment, i.e., decreasing C_{OHC} .

Eq. (B3) for a given BF. The CA gain also determines the strength of BM compression [see Fig. 4(b)] and two-tone rate suppression (Zhang *et al.*, 2001).

III. MODELING THE IMPAIRED AUDITORY PERIPHERY

A. Modeling OHC impairment

In order to model the effects of OHC status on the nonlinear BM filter, we introduce a scaling constant C_{OHC} to the output of the control path, such that

$$\tau_{\text{sp_impaired}}[n] = C_{\text{OHC}}(\tau_{\text{sp}}[n] - \tau_{\text{wide}}) + \tau_{\text{wide}}, \quad (8)$$

where $0 \leq C_{\text{OHC}} \leq 1$. The effects of C_{OHC} on the tuning of the signal-path filter at its narrowest bandwidth and largest gain ($\tau_{\text{sp}} = \tau_{\text{narrow}}$) are shown in Fig. 1(b).¹

The effects of C_{OHC} on tuning curves are illustrated in Fig. 4(a) for model fibers at two different BFs. To model normal OHC function, C_{OHC} is set to 1 and consequently the filter behavior is normal: tuning curves are narrow and thresholds are low. The upward “notches” in the tuning curves just above 4 kHz are due to the notch in the ME filter [see Fig. 19(b)]. The effects of C_{OHC} on compression are shown in Fig. 4(b) for one model fiber. With $C_{\text{OHC}}=1$ the BM filter exhibits compression for a BF tone from ~ 30 dB SPL to >100 dB SPL. Not shown here, the model also exhibits two-tone suppression due to the behavior of the wideband non-linear filter (Zhang *et al.*, 2001), which is also apparent in responses to vowel stimuli (see Sec. IV).

To model impaired OHC function, C_{OHC} is set to some value between 1 and 0; the lower the value, the greater the impairment. Reducing C_{OHC} causes two changes in the filter behavior.

First, the effect when the control path signal is small (i.e., at low sound levels) is to increase the tuning curve bandwidth and elevate thresholds around BF. Thresholds in the low-frequency “tail” of the tuning curve decrease slightly with increasing impairment. This behavior is qualitatively consistent with physiological reports of hypersensitive tails in tuning curves with OHC impairment (Liberman and Dodds, 1984a). In addition, a small downward shift in BF is observed in Fig. 4(a) for the model fiber with an unimpaired BF of 2.5 kHz; we refer to this shifted-BF following impairment as the “impaired BF.” The shift is due to the effects of the ME filter and IHC LP filter on the tuning curve shape, not a change in the BM filter’s center frequency, and only occurs in the steep transition bands of the ME and IHC filters. Upward shifts of less than 0.15 oct occur for unimpaired BFs less than 0.5 kHz (i.e., in the high-pass transition band of the ME filter) and between ~ 4.2 and 5.0 kHz (i.e., in the upper edge of the ME notch); downward shifts of less than 0.35 oct occur for unimpaired BFs between ~ 1.3 and 4.2 kHz (i.e., in the lower edge of the ME notch and the low-pass transition band of the IHC filter). Physiological data show shifts in the BM filter’s center frequency at high intensities or with impairment (e.g., Robles and Ruggero, 2001) that are larger than those seen in this model.

Second, when the control path signal is significant (i.e., at moderate to high stimulus intensities), compression and suppression are reduced because of the scaling down of the time-varying component of $\tau_{\text{sp}}[n]$ [Fig. 4(b)]. The extreme case of $C_{\text{OHC}}=0$ describes complete loss of OHC function: tuning curves are at their highest and broadest and compression and suppression are completely lost. Figure 4(b) shows that for a BF of 2.5 kHz the normal model produces a cochlear-amplifier gain of ~ 46 dB SPL, as prescribed by Eq. (B3).

B. OHC impairment as a function of BF

In order to predict data from populations of AN fibers, we must have estimates of the levels of OHC and IHC impairment as a function of BF. As described by Liberman and Dodds (1984a) and modeled in Fig. 4, damage to the OHCs causes both an increase in thresholds and a broadening in tuning. However, damage to the IHCs also leads to elevated

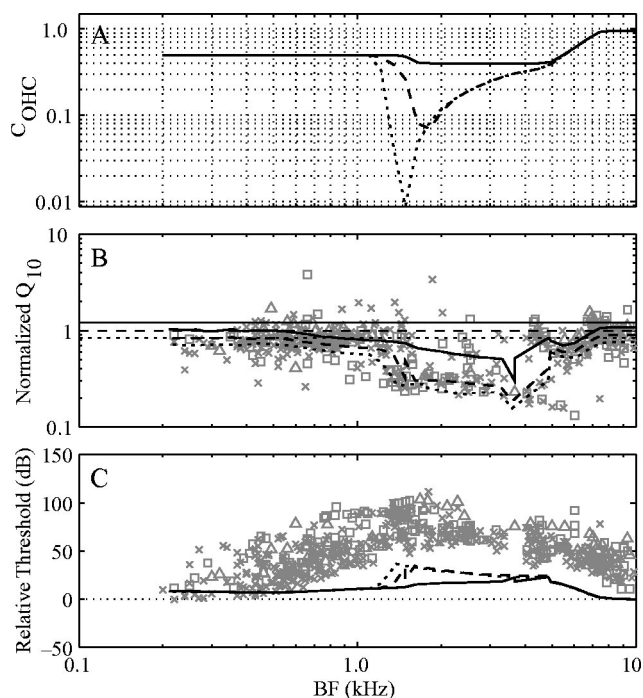


FIG. 5. Determination of model OHC impairment to fit impaired Q_{10} values as a function of BF. (a) Three different functions for C_{OHC} versus unimpaired BF to produce mild (solid line), moderate (dashed line), and severe (dotted line) OHC impairment as shown by the corresponding lines in (b). Definitions of these three cases are given in the text. (b) Impaired Q_{10} versus impaired BF, with Q_{10} values normalized by a linear fit to the normal-cat data plotted in Fig. 3. Gray symbols indicate data from individual fibers and thick lines indicate model predictions given the three functions for C_{OHC} shown in (a). Thin lines show the 75th, 50th, and 25th percentile of the normal data when normalized by the linear fit. (c) Impaired threshold versus impaired BF, where threshold values are given relative to the respective normal best threshold curves for the data and model. Gray symbols indicate data from individual fibers and lines indicate the model predictions given the functions for C_{OHC} shown in (a).

thresholds (Liberman and Dodds, 1984a), and therefore the increase in thresholds is not an uncontaminated indicator of the degree of OHC impairment. In contrast, Q_{10} values are not thought to be affected greatly by IHC impairment (Liberman and Dodds, 1984a). The following method is used in Secs. IV A, IV B, and IV D to model data from single impaired AN fibers. First, we set the value of τ_{narrow} in the model using the Q_{10} value of an example *normal* fiber with approximately matching BF. Second, we find a value for C_{OHC} that explains the estimated Q_{10} value of the example *impaired* fiber. Third, we apply enough IHC impairment (see Sec. III C) to explain the remaining threshold shift not accounted for by the OHC impairment.

In Sec. IV C, functional relationships between C_{OHC} and BF are derived to allow modeling of data from populations of AN fibers. Three functions are used, which are designed to follow the 75th, 50th, and 25th percentiles of the Q_{10} data from Miller *et al.* (1997). Figure 5(b) shows the Q_{10} data from impaired animals normalized by the best fit log-log line from normal animals (Fig. 3). The three horizontal lines show the 75th, 50th, and 25th percentiles of the normal data. The decrease in Q_{10} data points below the lines are a result of acoustic trauma. Figure 5(a) shows three empirical C_{OHC} functions designed to fit the 75th, 50th, and 25th percentiles of the impaired data. In doing these fits, the normal model fit

to the 75th percentile line of the normal data was adjusted to fit the 75th percentile of the impaired data by varying C_{OHC} , and similarly for the 50th and 25th percentiles. The three lines that follow the data points in Fig. 5(b) show the resulting Q_{10} 's for model tuning curves. The irregularities in the model Q_{10} values between 3 and 5 kHz result from the ME notch.

The threshold shifts resulting from the model OHC impairment are shown in Fig. 5(c). Even severe OHC impairment, as derived from the Q_{10} data, can at best account for around two-thirds of the threshold shift seen in the impaired-cat data; we postulate that the remainder should be attributed to IHC damage. Miller *et al.* (1997) found that fibers with BFs near the exposure frequency were under-represented in the impaired cats, relative to the normal cats, and argued for substantial IHC damage, followed by silencing and perhaps degeneration of some AN fibers. Fibers with less severe IHC damage should still be responsive to acoustic stimuli but with elevated thresholds. Modeling of such IHC impairment is described next.

C. Modeling IHC impairment

Elevated threshold tuning curves due to IHC impairment can be modeled by decreasing the slope of the function that relates BM vibration to IHC potential [the block IHC NL in Fig. 1(a)]. At the same time, the saturation potential must remain the same to retain maximum discharge rates close to those of normal fibers (e.g., Liberman and Kiang, 1984; Miller *et al.*, 1999a). Both of these effects can be achieved together in the model by decreasing the slope of the IHC NL block, or equivalently by scaling down the output of the narrow-band BM filter at the input of the IHC nonlinearity using a scaling constant C_{IHC} , where $0 \leq C_{\text{IHC}} \leq 1$. A value of one produces normal IHC function and a value of zero gives total IHC disfunction. To model individual example fibers, a value for C_{IHC} is chosen that accounts for the threshold shift not explained by OHC impairment.

Figure 6(a) shows the values of C_{IHC} that are needed to explain the minimum threshold shift in the AN population data not accounted for by the OHC impairment of Fig. 5(a). Figure 6(b) shows the threshold shifts as a function of impaired BF resulting from the IHC impairment in panel (a) in combination with the three cases of OHC impairment from Fig. 5 (heavy lines). The combined threshold shifts match the minimum threshold shifts in the data reasonably well. Minimum rather than average thresholds are fit because we assume that the distribution of thresholds at any given BF reflects variation in synapse gain, i.e., the difference between low and high spontaneous rate AN fibers (Geisler, 1981; Heinz *et al.*, 2001). Consistent with the data of Liberman and Dodds (1984a), Q_{10} values are relatively unaffected by IHC impairment in the model, although tuning at levels 20 dB or greater above threshold is broadened due to the broadened filtering of the normal BM at higher stimulus levels.

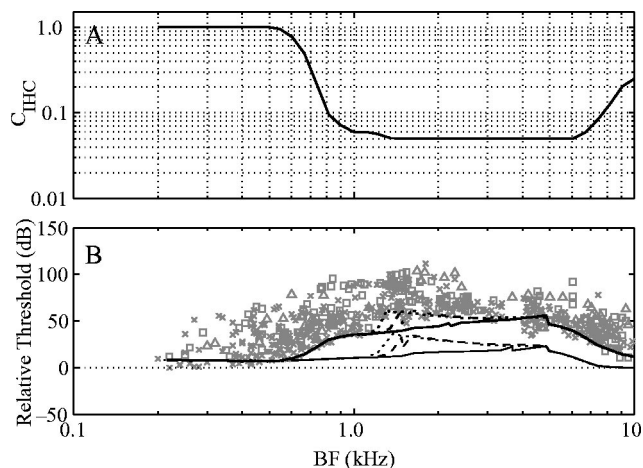


FIG. 6. Determination of model IHC impairment to fit minimum threshold shifts as a function of BF. (a) Function for C_{IHC} versus unimpaired BF to produce the threshold shifts as shown in panel (b). (b) Impaired thresholds relative to the respective normal best threshold curves for the data and model versus impaired BF. Gray symbols show data from individual fibers and thin lines show threshold shifts for OHC impairment alone (replotted from Fig. 5). The thick lines show the model threshold shifts with IHC impairment as described in panel (a) in combination with the three cases of OHC impairment: mild (solid line), moderate (dashed line), and severe (dotted line).

IV. SYNCHRONIZED RESPONSE TO THE VOWEL /ε/

A. Single-fiber data and predictions

Miller *et al.* (1997) recorded AN single-fiber responses to the synthesized vowel /ε/ with the spectrum shown in Fig. 7. This synthesized vowel is periodic with a fundamental frequency (F_0) of 100 Hz and formant frequencies (F_1 - F_5) of 0.5, 1.7, 2.5, 3.3, and 3.7 kHz. Note that the stimulus has been filtered by the head related transfer function (HRTF) of a human head (Wiener and Ross, 1946).

The synchronized responses of AN fibers to an ~80 ms vowel stimulus were evaluated by taking the Fourier transform of the poststimulus time histogram (PSTH) normalized to units of spikes/second (Miller *et al.*, 1997). Synchronized rates for two fibers with BFs near F_2 are plotted in Fig. 8. At the lowest presentation level [panel (c)], the normal fiber responds to a number of frequency components of the vowel

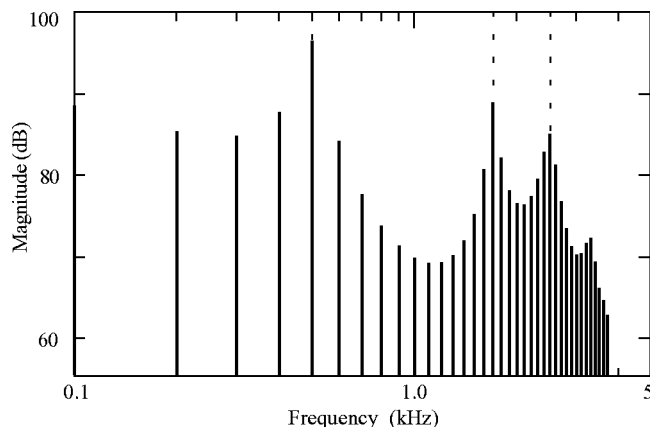


FIG. 7. Power spectrum of the vowel /ε/ used in the physiological experiments. Modified from Fig. 1 of Miller *et al.* (1997) with permission from the Acoustical Society of America® (1997).

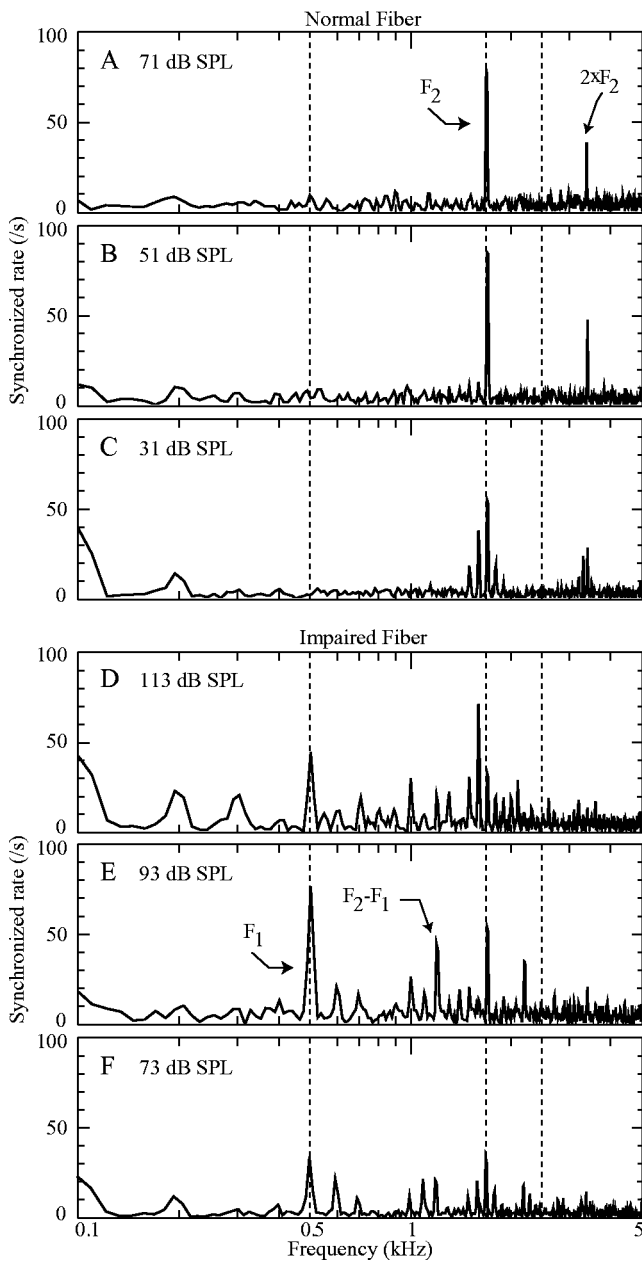


FIG. 8. Synchronized response of a normal [(a)–(c)] and an impaired [(d)–(f)] fiber, both with BFs around F_2 , to the vowel / ϵ /. Synchronized rate is the magnitude of the Fourier transform of a PSTH (binwidth $20 \mu\text{s}$), with units of spikes/s. The normal fiber had a BF of 1.7 kHz and a Q_{10} of 4.4, and the impaired fiber had a BF of 1.6 kHz, a threshold shift of ~ 60 dB, and a Q_{10} of 3.8. Reprinted from Fig. 9 of Miller *et al.* (1997) with permission from the Acoustical Society of America © (1997).

in the spectral peak around F_2 . This fiber exhibits synchrony capture at the two higher stimulus levels [panels (a) and (b)]: as the stimulus level increases above the fiber threshold, the responses becomes synchronized almost exclusively to the vowel component at F_2 . In contrast, the impaired fiber [(d)–(f)] shows a much more broadband response, particularly to the higher-intensity first formant. Note the higher presentation levels used to compensate for the elevated threshold of this impaired fiber.

Shown in Fig. 9(a) are synchronized responses of a model fiber with normal OHC and IHC function ($C_{\text{OHC}} = C_{\text{IHC}} = 1$); the BF, threshold, and Q_{10} approximately

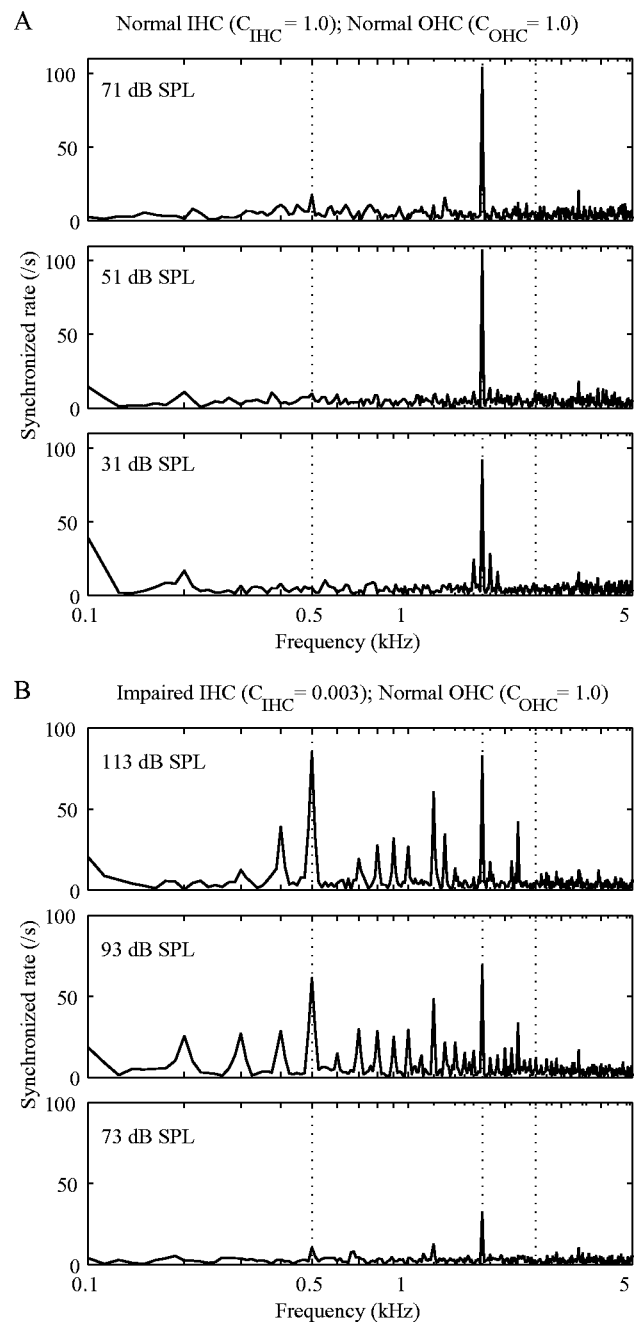


FIG. 9. Model predictions of a low-frequency (BF $\approx F_2$) AN fiber's synchronized response to the vowel / ϵ /. (a) Normal OHC and IHC ($C_{\text{OHC}} = C_{\text{IHC}} = 1$); BF = 1.7 kHz. (b) Severely impaired IHC ($C_{\text{IHC}} = 0.003$) and normal OHC ($C_{\text{OHC}} = 1$); unimpaired BF = 1.7 kHz, impaired BF ≈ 1.6 kHz, threshold shift ≈ 60 dB, and impaired $Q_{10} \approx 3.8$.

match those of the normal fiber from Fig. 8. Like the normal fiber of Fig. 8, the model fiber synchronizes to a number of vowel components around the F_2 spectral peak at the lowest stimulus intensity (31 dB SPL) and almost exclusively to the F_2 component at the higher intensities. Also observed is a synchronized response to the second harmonic of F_2 , although it is somewhat smaller than that of the example normal fiber. The major cause of the synchrony capture by F_2 at the higher intensities is the compressive/suppressive nonlinearity of the signal-path, narrow-band BM filter. At the 31 dB SPL presentation level, around 82% of the signal power at the output of the narrow-band BM filter is at the F_2 fre-

quency; the narrow-band filter is effectively linear at this presentation level [Fig. 4(b)]. At 51 and 71 dB SPL, the narrow-band filter is operating in its nonlinear range, causing the percentage of the signal power at $F2$ to increase to 89% and 92%, respectively. These percentage values are relatively unaffected by further processing of the signal by the IHC, synapse, and spike generator sections of the model.

The example impaired fiber of Figs. 8(d)–(f) presents an interesting case: it has relatively normal pure-tone tuning as measured by Q_{10} values but has a broadband synchronized response to the vowel (Miller *et al.*, 1997). How could this come about? Shown in Fig. 9(b) are synchronized responses of a model fiber with severely impaired IHC function ($C_{\text{IHC}}=0.003$) and normal OHC function ($C_{\text{OHC}}=1$); the impaired BF, threshold shift, and Q_{10} approximately match those of the impaired fiber from Fig. 8. The model predictions are consistent with the data plotted in Figs. 8(d)–(f), showing synchrony to many frequency components of the vowel (i.e., loss of synchrony capture), including a particularly large response to $F1$. Examination of the output of each stage of the model's signal path shows how synchrony capture is lost without impairment to the BM filter. As stated above, around 92% of the signal power at the output of the narrow-band BM filter is at the $F2$ frequency for a presentation level of 71 dB SPL. This percentage value drops to only 59% if the presentation level is increased to 93 dB SPL, because at this level the narrow-band BM filter tuning is very broad [see Fig. 1(b)] and its gain is fairly linear again [see Fig. 4(b)]. However, with normal IHC function the signal at the output of the narrow-band BM filter is so large that it falls within the nonlinear (saturating) ranges of the IHC nonlinearity and the synapse model. Saturation of the signal suppresses the smaller frequency components such that the percentage of the signal power at $F2$ increases to 80% at the output of the IHC and 91% at the output of synapse model. That is, synchrony capture is lost at the narrow-band BM filter at high presentation level but is regained through the nonlinear processing of the normal IHC and synapse. When the IHC is impaired, the signal no longer saturates the IHC nonlinearity and synapse model, and the percentage of the signal power at $F2$ drops to 38% at the output of the IHC and 27% at the output of the synapse model, producing the broadband synchrony observed in Fig. 9(b). These results show that loss of synchrony capture at high stimulus levels can be produced solely by IHC impairment, with no impairment of BM tuning necessary.

OHC impairment alone can also give rise to broadband synchrony at some stimulus levels. Results are shown in Fig. 10(a) for a model fiber with BF matching the example impaired fiber of Fig. 8, but with normal IHC function ($C_{\text{IHC}}=1$) and total OHC impairment ($C_{\text{OHC}}=0$). At the lower two presentation levels the impaired BM response is broad enough to create broad synchrony in the model AN fiber. In these cases, the BM response is broader and more linear than for the normal BM, and the reduced gain of the BM means that the signal falls more within the linear regions of the IHC nonlinearity and the synapse model, as was the case for IHC impairment. At the highest level the signal is large enough for the IHC and synapse to produce synchrony capture to $F2$

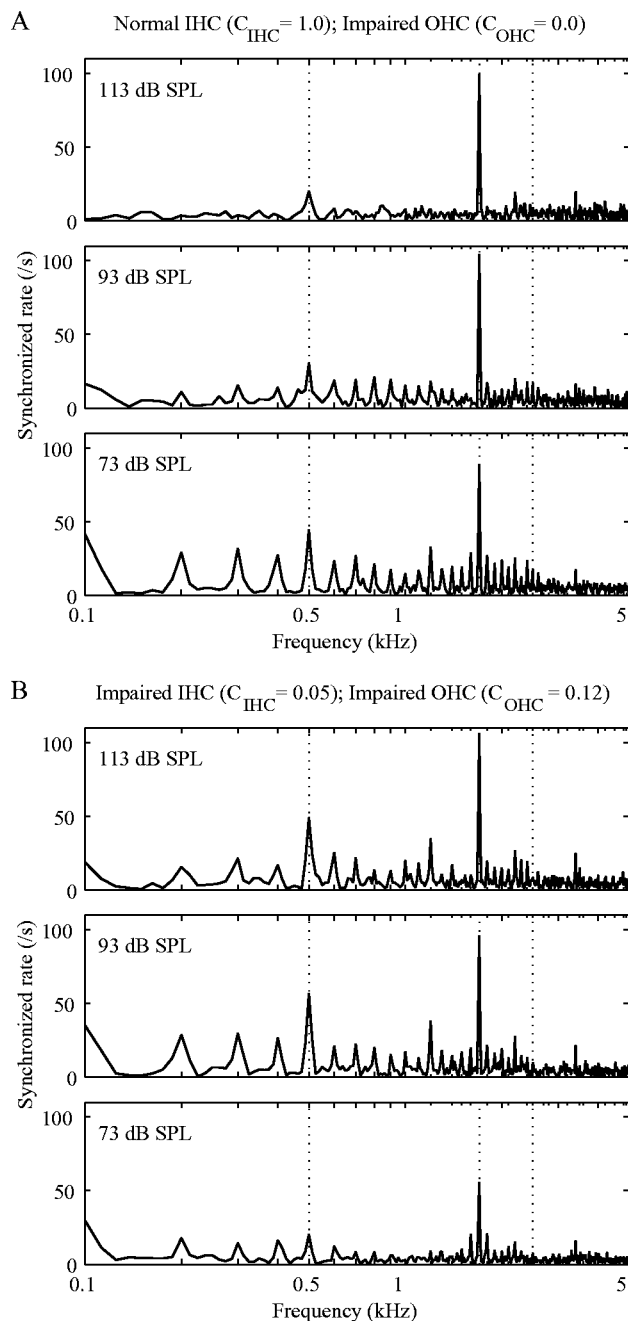


FIG. 10. Model predictions of a low-frequency ($\text{BF} \approx F2$) AN fiber's synchronized response to the vowel / ϵ /. (a) Totally impaired OHC ($C_{\text{IHC}}=0$) and normal IHC ($C_{\text{IHC}}=1$). (b) Moderately impaired OHC ($C_{\text{OHC}}=0.12$) and impaired IHC ($C_{\text{OHC}}=0.05$).

once again. This illustrates how in some cases synchrony capture can occur without suppression at the level of the BM. A more typical situation is combined IHC and OHC impairment like that discussed in Fig. 6. Moderate OHC impairment ($C_{\text{OHC}}=0.12$) combined with IHC impairment ($C_{\text{OHC}}=0.05$) produces broadband synchrony at all presentation levels [Fig. 10(b)].

The effects of combined IHC and OHC impairment can also be observed for fibers with BFs in the $F3$ region. Synchronized rates for two fibers from Miller *et al.* (1997), one normal and one impaired, with BFs near $F3$ are plotted in Fig. 11. Limited synchrony capture is observed in this nor-

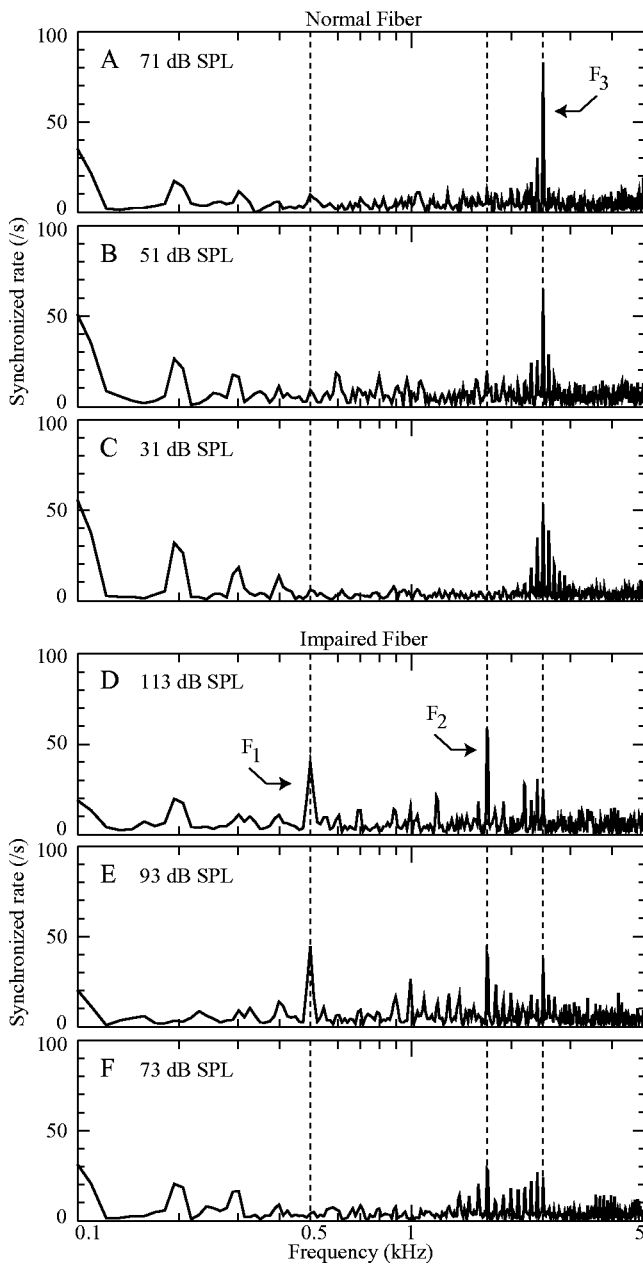


FIG. 11. Synchronized response of a normal [(a)–(c)] and an impaired [(d)–(f)] fiber, both with BFs around F_3 , to the vowel /ε/. The normal fiber had a BF of 2.5 kHz and a Q_{10} of 4.3, and the impaired fiber had a BF of 2.6 kHz, a threshold shift of ~ 60 dB, and a Q_{10} of 1.4. Reprinted from Fig. 10 of Miller *et al.* (1997) with permission from the Acoustical Society of America © (1997).

mal fiber [(a)–(c)]; synchrony capture is not observed in most normal fibers with BFs near F_3 , although they do exhibit a strong response to F_3 . The impaired fiber [(d)–(f)] again shows much broader tuning, synchronizing particularly to F_1 and F_2 , with little response to F_3 .

Shown in Fig. 12(a) are synchronized responses of a model fiber with normal OHC and IHC function ($C_{\text{OHC}} = C_{\text{IHC}} = 1$); the BF, threshold and Q_{10} approximately match those of the normal fiber from Figs. 11(a)–(c). The model fiber synchronizes predominantly to frequency components around its BF, consistent with the example normal fiber, although it does not show the same degree of synchrony capture at the highest presentation level. Results are shown in

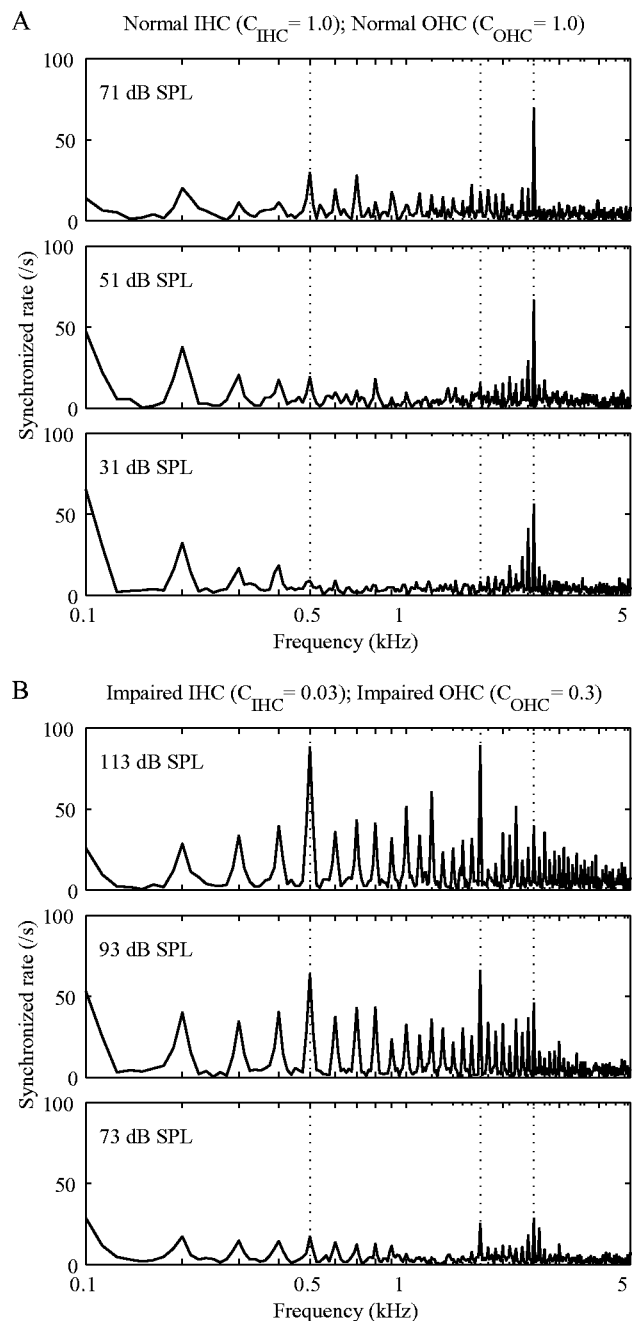


FIG. 12. Model predictions of a moderate-frequency (BF $\approx F_3$) AN fiber's synchronized response to the vowel /ε/. (a) Normal IHC and OHC ($C_{\text{IHC}} = C_{\text{OHC}} = 1$). (b) Impaired IHC ($C_{\text{IHC}} = 0.03$) and impaired OHC ($C_{\text{OHC}} = 0.3$); unimpaired BF = 2.93 kHz, impaired BF ≈ 2.6 kHz, threshold shift ≈ 60 dB, and impaired $Q_{10} \approx 1.4$.

Fig. 12(b) for a model fiber with impaired IHC ($C_{\text{IHC}} = 0.03$) and OHC ($C_{\text{OHC}} = 0.3$) function; the impaired BF, threshold shift, and Q_{10} approximately match those of the impaired fiber from Figs. 11(d)–(f). Like the example fiber, the impaired model fiber exhibits broadband synchrony to the vowel, particularly to the lower-frequency formants F_1 and F_2 , although the synchrony to nonformant harmonics is larger in the model fiber.

B. Quantitative assessment of synchrony capture

Wong *et al.* (1998) quantified synchrony capture using power ratios (PRs), which subdivide the response into com-

ponents related to the formants and other components. Total power is the sum of the squares of the synchronized rates $R(kf_0)$ over the first 20 harmonics of the stimulus. The $F2$ PR is the fraction of the total power that is phase-locked to the second formant (the 17th harmonic). $F1$ & $F2$ -related power is the sum of the squares of the synchronized rates at the harmonics related to $F1$ and $F2$, which include the 5th ($F1$), 7th ($F2 - 2 \times F1$), 10th ($2 \times F1$), 12th ($F2 - F1$), 15th ($3 \times F1$), 17th ($F2$), and 20th ($4 \times F1$); the distortion products are included in the $F1$ & $F2$ response because they most likely result from rectifier distortion in the IHC-AN synapse (Young and Sachs, 1979). The $F1$ & $F2$ -related PR is the fraction of the total power contained in the $F1$ & $F2$ -related harmonics.

Wong *et al.* (1998) measured power-ratios in AN fibers in response to a 400-ms synthetic vowel with a spectrum identical to that of the / ϵ / vowel stimulus shown in Fig. 7, except that the sampling rate was adjusted so that $F2$ always fell at the BF of the fiber. Example power-ratio data from Wong *et al.* (1998) are shown in the left column of Fig. 13 for four normal fibers with different BFs as labeled. These data reveal a breakdown in synchrony capture by $F2$ at very high sound levels, where significant response to $F1$ occurs at the expense of response to $F2$. In the left column of Fig. 13, fiber A exhibits synchrony capture by $F2$ (dashed line) at all stimulus levels. Fiber B exhibits synchrony capture by $F2$ at moderate stimulus levels, which is lost at very high levels (≥ 80 dB SPL). When the $F2$ PR drops, the $F1$ & $F2$ PR (solid line) stay the same, showing that the $F2$ response is replaced by a response to $F1$. Fibers C and D have progressively lower intensities at which the transition from $F2$ to $F1$ synchrony begins. This tendency occurs consistently as BF increases (Wong *et al.*, 1998). The lower and upper bounds of the shaded regions in the left column of Fig. 13 represent, respectively, the sound levels at which synchrony capture by $F2$ is lost, meaning the vector strength $VS(F2) = |R(F2)|/R(0) < 0.5$, and the component-2 (C2) threshold for $F1$ (Liberman and Kiang, 1984). The C2 threshold is the stimulus level at which a substantial phase change occurs in the synchronized response (see Fig. 1 of Wong *et al.*, 1998) and is thought to correspond to a change in the mode of stimulation of the fiber. Modeling the component-1 (C1) to C2 transition for pure-tone stimuli has been accomplished using a dual-path BM filter (e.g., Goldstein, 1990; Schoonhoven *et al.*, 1994; Meddis *et al.*, 2001), not included in this model.

Predictions have been obtained for model fibers with BFs roughly covering the range of BFs in the Wong *et al.* (1998) data. Consistent with the physiological data, the model predictions for normal IHC and OHC function ($C_{IHC} = C_{OHC} = 1$) shown in the right column of Fig. 13 exhibit synchrony capture by $F2$ at moderate sound levels (< 70 dB SPL in all cases). One factor that is crucial in producing synchrony capture by $F2$ at moderate sound levels is the high-pass filtering of the ME below 1 kHz; without ME filtering, $F1$ [< 1 kHz for all the Wong *et al.* (1998) stimuli] also produces a strong response at moderate intensities.

Also seen in the model predictions in the right column of Fig. 13 is the transition in synchrony from $F2$ to $F1$ at

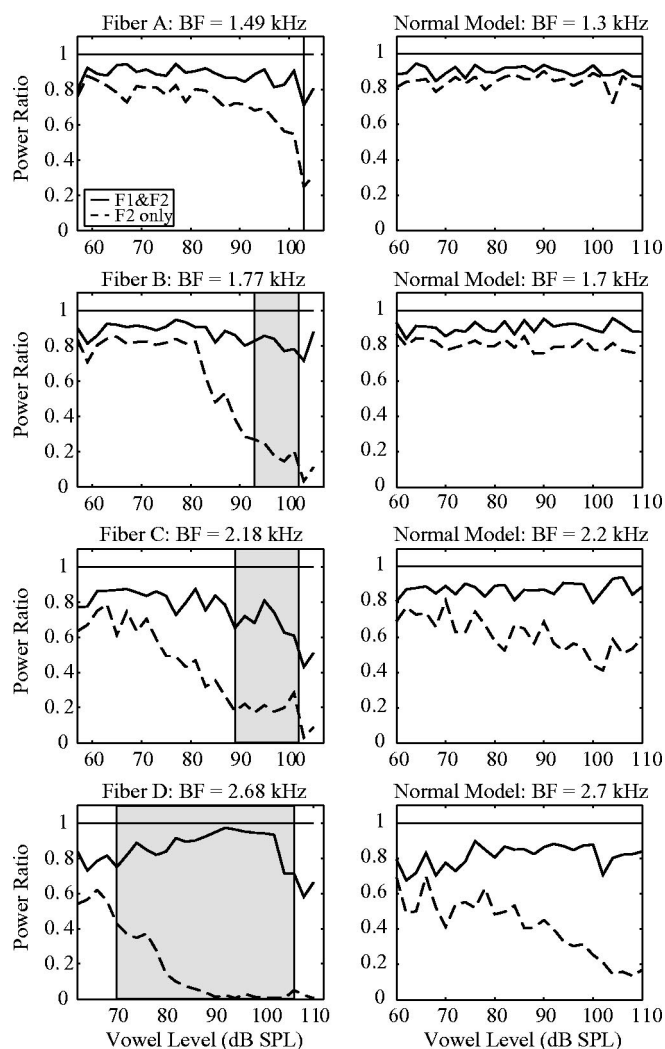


FIG. 13. Normal power ratio data at high sound levels. Left column: four normal fibers with BFs as labeled, redrawn from Fig. 4 of Wong *et al.* (1998) with permission from Elsevier Science[©] (1998). The solid and dashed lines, respectively, show the fraction of total power in the fiber's response that is synchronized to $F1$ and $F2$ combined ($F1$ & $F2$) or to $F2$ alone. The lower and upper bounds of the shaded regions represent, respectively, the sound levels at which a loss of synchrony capture by $F2$ occurs and the component 2 threshold for $F1$. Right column: four normal model fibers with BFs as labeled.

higher intensities, although the effect is weaker than in the data and the stimulus intensity at which the switch occurs does not appear to decrease with increasing BF. Wong *et al.* (1998) argued that the lower-level switch from $F2$ to $F1$ synchrony with increasing BF is likely due to the increasing strength of two-tone suppression with increasing BF. This effect is partly represented in the model by the increase in cochlear-amplifier gain with BF (Fig. 20). Reducing the gain for a model fiber with $BF = 2.7$ kHz to the gain prescribed for a model fiber with $BF = 1.3$ kHz greatly reduces the switch in synchrony at high intensities (results not shown). In addition, there is a small secondary factor not considered by Wong *et al.* (1998), which is that with increasing BF, the frequency-scaled vowel has an increasing ratio of power at the $F1$ frequency relative to power at the $F2$ frequency, because $F1$ is attenuated less by the ME filter. This effect

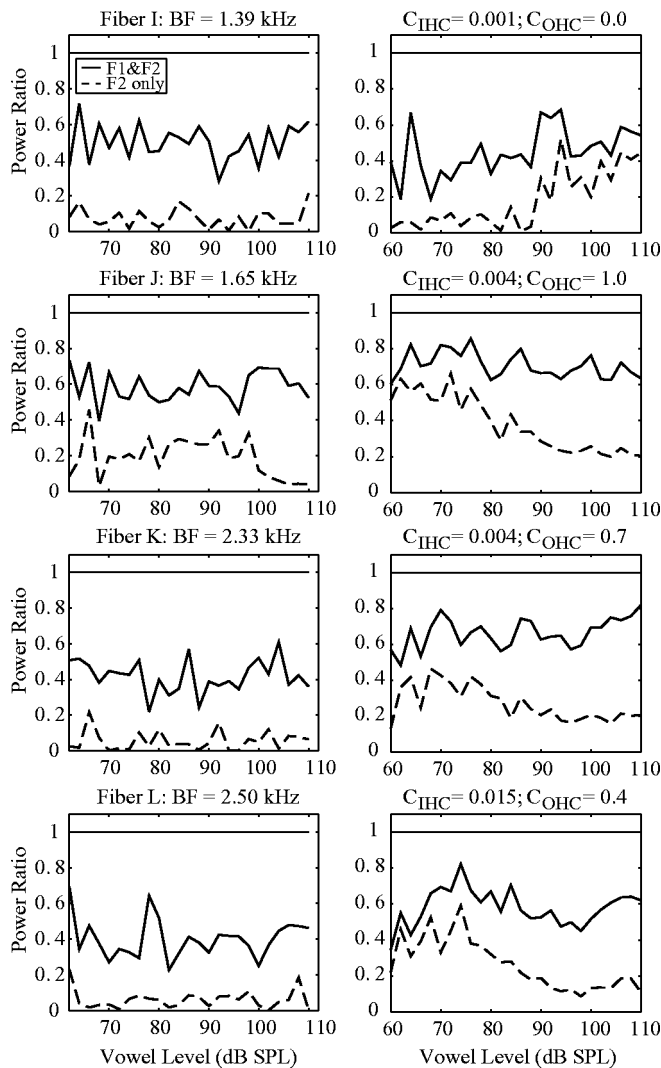


FIG. 14. Power ratio data for impaired fibers at high sound levels. Left column: four fibers exhibiting threshold shifts, with BFs as labeled, redrawn from Fig. 6 of Wong *et al.* (1998) with permission from Elsevier Science[®] (1998). Right column: four impaired model fibers (IHC and OHC impairment for each as labeled) with BFs of 1.3, 1.7, 2.2, and 2.7 kHz, respectively.

produces a slightly weaker response to F_2 at the highest intensities.

During the course of Wong *et al.*'s experiments, the high presentation levels caused threshold shifts in a number of fibers. The left column of Fig. 14 shows that in four fibers exhibiting threshold shifts, with different BFs as labeled, the synchrony to F_2 is low at all levels ($PR \approx 0.1-0.2$) and is only partly shifted to F_1 ; around 40%–50% of the synchrony is lost to other components of the vowel, as was observed in Figs. 8(d)–(f) and 11(d)–(f).

While the threshold shifts in the Wong *et al.* (1998) experiments may be temporary and therefore different in mechanism from permanent acoustic trauma (Liberman and Mulroy, 1982; Gao *et al.*, 1992; Nordmann *et al.*, 2000), it is of interest to see how IHC and OHC impairment as modeled in this paper predict the synchrony data in the left column of Fig. 14. Plotted in the right column of Fig. 14 are results from the four model fibers of Fig. 13 with individual IHC and OHC impairment as indicated in the figure. These im-

pairments give rise to thresholds and Q_{10} values approximately matching those of the four example fibers in the left column of Fig. 14. The model predicts the broadband synchrony (loss of synchrony to F_1 & F_2) seen in the data. The loss of synchrony to F_2 alone is fairly well described for some vowel presentation levels but not for others. Example fiber I (top-left panel in Fig. 14) has an extremely broad and elevated tuning curve (threshold ≈ 90 dB SPL; see Fig. 6 of Wong *et al.*, 1998), suggesting that only a C2 response remains in this impaired fiber. The model fiber with similar BF (top-right panel in Fig. 14) has a sharper tuning curve than the example fiber, even with C_{OHC} set to zero, because the model can only describe C1 responses. Consequently, the model exhibits some synchrony to F_2 at high presentation levels, which is not seen in the experimental data. The other three model fibers with BFs of 1.7, 2.2, and 2.7 kHz (right column in Fig. 14) are set to have relatively normal OHC function because of the fairly sharp tuning curve tips of example fibers J, K, and L (left column in Fig. 14). The model BM nonlinearity (compression and suppression) produces higher synchrony to F_2 at moderate presentation levels than is observed in the example fibers, suggesting that the example fibers may be subject to less compression and suppression than the model predicts from the tuning curves. These inaccuracies in the model predictions show the limitations in setting model OHC and IHC impairment to match individual experimental tuning curves.

C. Synchrony capture versus BF

Miller *et al.* (1997) measured F_1 , F_2 , and F_3 PRs in a population of fibers across a range of BFs. Model predictions of PRs for F_1 , F_2 , and F_3 are plotted as a function of BF in Fig. 15 for normal fibers and in Fig. 16 for impaired fibers. Following Miller *et al.* (1997), PRs here include the phase-locked response to the first, second, and third harmonics of the formant frequency, as long as the frequency of the harmonic is less than or equal to 5 kHz. Lines show model predictions and gray hatched areas indicate the range of values observed in the physiological data of Miller *et al.* (1997).

The model predictions for normal fibers (Fig. 15) fall predominantly within the range of values seen in the physiological data at both presentation levels (69 and 49 dB SPL). Normal fibers synchronize almost exclusively to the formant frequency closest to their BFs. The small peak in the F_1 PR of the model predictions at 1 kHz ($2 \times F_1$) is due to harmonic distortion in the nonlinear BM filter. Such harmonic distortion of F_1 is also observed in the physiological data at 69 dB SPL but is not apparent in the data at 49 dB SPL.

With impaired IHC and OHC function (Fig. 16), model predictions of PRs fall within the range of single-fiber values for F_1 and F_3 , but not for F_2 . At both levels (112 and 92 dB SPL), synchrony to F_2 is overestimated in the BF region around F_2 —possible causes are examined in Sec. V. A second discrepancy is observed at the higher presentation level (112 dB SPL): an upward shift in the peak of F_1 synchrony is observed in the data when compared to the lower presentation level (92 dB SPL). This shift is seen in the model predictions but is less pronounced.

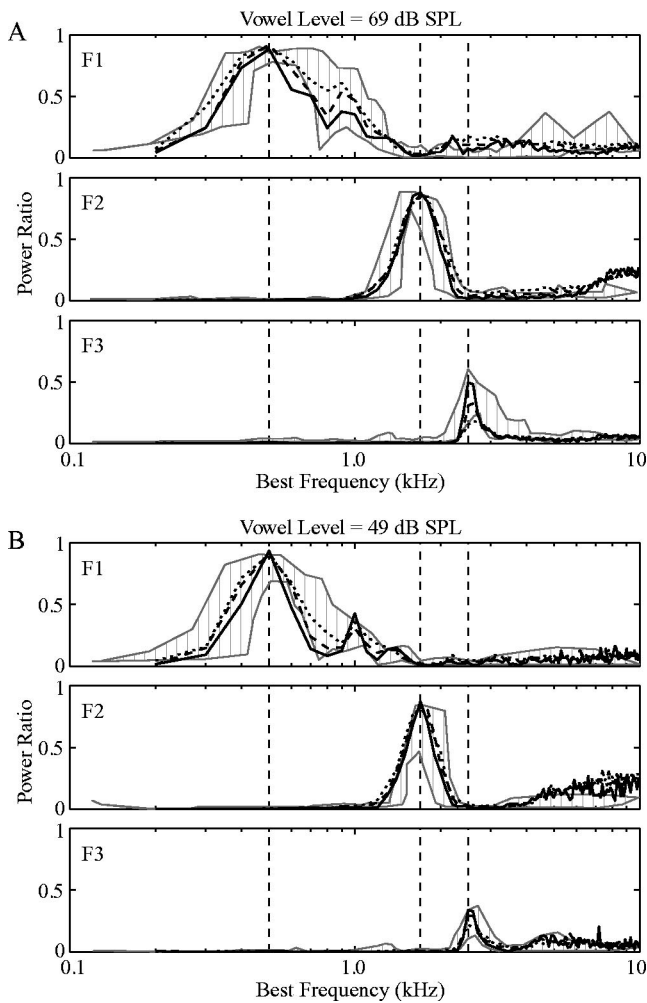


FIG. 15. Model predictions of normal power ratios for $F1$, $F2$, and $F3$ as a function of BF for stimulus intensities of 69 dB SPL (a) and 49 dB SPL (b). Thick lines show model predictions and gray hatched areas indicate the range of values observed in the normal physiological data of Miller *et al.* (1997). Vertical dashed lines show the formant frequencies. Predictions are shown for model Q_{10} values that are at the 75th (solid lines), 50th (dashed lines), and 25th (dotted lines) percentiles of Q_{10} values for the physiological data.

D. Signal processing to restore synchrony capture

In Schilling *et al.* (1998) and Miller *et al.* (1999a), two different amplification schemes were investigated for their potential to restore normal BF-dependent pattern of synchrony capture for the vowel / ϵ / in acoustically traumatized cats. Schilling *et al.* (1998) tested a common hearing-aid processing scheme, where the amplification has a frequency-shaped gain function in which the gain is larger in regions of greater threshold shift. They found that this amplification scheme did indeed restrict the upward spread of synchrony to $F1$ when compared to flat amplification. However, it could not prevent the upward spread of synchrony to $F2$ and $F3$. Perhaps more importantly, there was a strong and inappropriate synchrony of fibers with BFs in the trough region (~ 1 kHz) between $F1$ and $F2$ to energy at their BFs. This response was presumably created by the low-frequency edge of the amplification gain function and, in a hearing impaired individual, could produce an anomalous perception of a for-

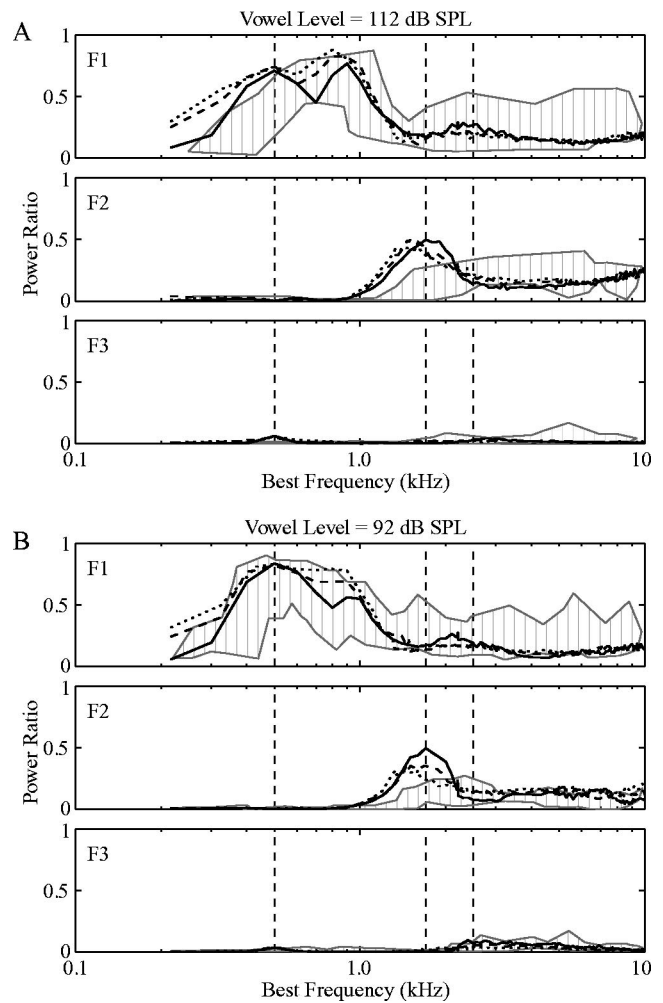


FIG. 16. Model predictions of impaired power ratios for $F1$, $F2$, and $F3$ as a function of impaired BF for stimulus intensities of 112 dB SPL (a) and 92 dB SPL (b). Thick lines show model predictions and gray hatched areas indicate the range of values observed in the impaired physiological data of Miller *et al.* (1997). Vertical dashed lines show the formant frequencies. Predictions are shown for model Q_{10} values that are at the 75th (solid lines), 50th (dashed lines), and 25th (dotted lines) percentiles of Q_{10} values for the impaired physiological data, i.e., for the three functions of C_{OHC} given in Fig. 5(a), and with IHC impairment as shown in Fig. 6(a).

mant, confounding the identification or discrimination of actual vowel formants.

To overcome this problem, Miller *et al.* (1999a) developed an alternative frequency-shaping scheme, contrast-enhancing frequency shaping (CEFS), where the edge of the gain profile is placed not at the frequency where thresholds begin to increase but rather just below the $F2$ frequency, creating a stronger contrast between $F2$ and the lower-frequency components such as $F1$ and the trough. The spectra of the standard and CEFS vowels are shown in Fig. 17. A 30 dB of gain has been applied to the frequencies above $F2$, to compensate for threshold shifts of around 60 dB in that region (see Lybarger, 1978, for an explanation of the “half gain rule”). The formant frequencies are identical to the previously described / ϵ / stimulus. In contrast to the previous stimulus, no HRTF filtering has been applied to the vowels in Fig. 17, so the $F3$ intensity is lower relative to $F2$, and both formant intensities are lower relative to $F1$.

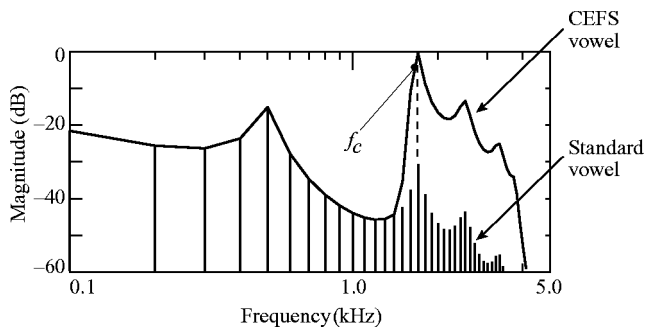


FIG. 17. Power spectra of the standard and CEFS versions of the vowel /ε/. The line spectrum shows the unprocessed vowel's spectral shape and the solid line shows the CEFS-modified spectral envelope. The CEFS vowel was obtained by high-pass filtering the standard vowel with a cutoff frequency f_c , which is 50 Hz below the second formant frequency (indicated by the vertical dashed line). Modified from Fig. 1(b) of Miller *et al.* (1999a) with permission from the Acoustical Society of America[®] (1999).

Shown in Fig. 18 are predictions for the CEFS vowel with the same impaired model fibers as in Figs. 9(b) and 12(b). The presentation levels for the CEFS vowel are 8 dB lower than those used in Figs. 9 and 12 so that the F_2 intensities are matched to those of the standard vowels. For a model fiber with parameters the same as for Fig. 9(b) (impaired IHC, normal OHC, and impaired BF=1.6 kHz $\approx F_2$), synchrony capture to F_2 is mostly regained with the CEFS vowel [Fig. 18(a); cf. normal data in Fig. 8(a)]. A model fiber with parameters the same as for Fig. 12(b) (impaired IHC, impaired OHC, and impaired BF=2.6 kHz $\approx F_3$) exhibits synchrony capture to the *second* formant of the modified vowel, instead of to F_3 [Fig. 18(b); cf. normal data in Fig. 11(a)]. The same undesirable effect is seen in the AN fiber data with CEFS amplification (see Figs. 10 and 11 of Miller *et al.*, 1999a).

V. DISCUSSION

A. Sources of changes in synchrony in acoustically traumatized cats

The model predictions presented in this paper suggest that both OHC and IHC impairment contribute to the degradation of the tonotopic representation of formant frequencies (i.e., BF-appropriate synchrony) in AN fibers damaged by acoustic trauma. OHC impairment broadens and linearizes BM tuning, thereby causing AN fibers to synchronize to many vowel components. This is consistent with the results of Geisler (1989), who used an AN model with a linear BM filter and found that broadened tuning led to an upward spread of synchrony to F_1 in a few example model fibers. Similar results were found by Sachs *et al.* (2002) with a model including a nonlinear BM filter. Geisler (1989) argued that IHC impairment was not necessary to explain physiological data from sound-damaged cochleae, in spite of histological data showing that the degree and extent (i.e., BF region) of damage to IHC stereocilia is typically equal to or greater than damage to OHC stereocilia (Liberman, 1984; Liberman and Dodds, 1984a, b) for a sound-exposure paradigm similar to that of Miller *et al.* (1997). Geisler (1989) modeled OHC impairment by directly fitting filter functions to impaired tuning curves, i.e., by independently varying the

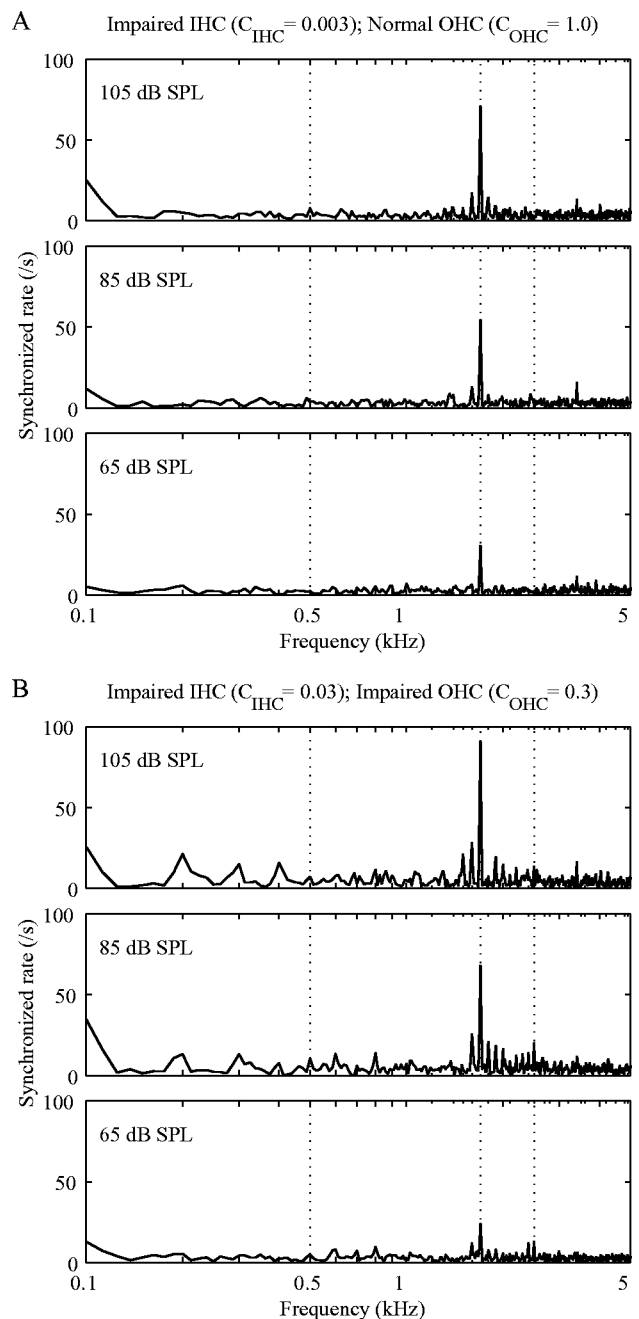


FIG. 18. Model predictions of responses to the CEFS vowel by impaired AN fibers. The presentation levels are reduced by 8 dB from those used for the standard vowel so that the levels of the F_2 components are matched for the CEFS vowel and the standard vowel. (a) Model fiber with parameters the same as for Fig. 9(b): impaired IHC ($C_{\text{IHC}}=0.003$) and normal OHC ($C_{\text{OHC}}=1$); impaired BF=1.6 kHz. (b) Model fiber with parameters the same as for Fig. 12(b): impaired IHC ($C_{\text{IHC}}=0.03$) and impaired OHC ($C_{\text{OHC}}=0.3$); impaired BF=2.6 kHz.

filter gain and bandwidth. However, our results suggest that some of the reduced gain in the Geisler (1989) filters may be better attributed to IHC impairment.

Our results show that IHC impairment *alone* can produce significant changes in the synchronized response to a vowel [see Fig. 9(b)]. The BM tuning is normally quite broad for high-intensity stimuli [see Fig. 1(b)], but normal IHC function leads to synchrony suppression of smaller vowel components. Synchrony capture caused by the IHC and the

IHC-AN synapse has also been illustrated in previous modeling studies (Schroeder and Hall, 1974; Geisler, 1985; Payton, 1988). The results of this paper add to these previous studies by suggesting over what range of stimulus intensities this occurs. As discussed in Sec. IV A, our model predicts that BM nonlinearity (compression and suppression) are the primary cause of synchrony capture for stimulus intensities between approximately 40 and 80 dB SPL, whereas IHC and synaptic nonlinearity (saturation) are the major cause of synchrony capture above 80 dB SPL. In the case of IHC impairment as modeled in Sec. III C, high-intensity signals fall within the linear region of the expanded IHC dynamic range and synchrony suppression is substantially reduced. In a similar fashion, the reduced BM gain in the case of OHC impairment causes the signal to fall within the linear region of the normal IHC dynamic range, leading to a reduction in synchrony suppression in the IHC, in addition to the already broader BM response. Note that the results described above are obtained only with a model including two-tone suppression. In the model of Carney (1993), which does not include any wideband nonlinearities in the BM filter, BM tuning remains relatively narrow even at high intensities and therefore IHC impairment has little effect. Without two-tone suppression, only broadening of BM tuning by OHC impairment causes any substantial change in the AN's synchrony to the vowel (Bruce *et al.*, 1999).

B. IHC impairment in acoustically traumatized cats

Geisler (1989) argued against the significance of IHC impairment for AN responses partly because a number of studies found relatively normal rate-level dynamic ranges for impaired fibers (e.g., Salvi *et al.*, 1983; Liberman and Kiang, 1984). The reasoning was that IHC impairment of the type we have modeled should decrease the slopes of rate-level functions, increasing their dynamic ranges (here slope is measured in a plot of rate versus log sound pressure, as dB). This is true in the model, in that the decrease in IHC gain increases the thresholds of AN fibers, which moves their dynamic ranges into the compression region of the BM input/output function [Fig. 4(b)], thus decreasing their slopes. The effect would, of course, be smaller for low spontaneous rate (high threshold) fibers, whose dynamic ranges normally incorporate more of the compression region (Sachs and Abbas, 1974; Yates, 1990). Computation of rate-level slopes for model fibers shows that, when level is expressed on a dB scale, the effect of IHC impairment with no OHC damage translates mainly into a threshold shift and the slopes with severe IHC impairment are approximately as shallow as normal low-spontaneous rate (high threshold) fibers (results not shown). OHC damage, of course has the opposite effect, either increasing or making no change in rate-level slopes, because OHC damage reduces the compression in the BM input/output function [Fig. 4(b)]. Increases in slope consistent with this expectation have been shown in AN fibers following OHC poisoning with kanamycin (Harrison, 1981) and similar changes are inferred from psychophysical masking experiments in hearing-impaired subjects (Oxenham and Plack, 1997). The opposite effects of IHC and OHC damage on rate-level slopes mean that, with the mixed losses in the

physiological data of Miller *et al.*, the effect on the slope of an individual AN fiber is difficult to predict and could be any of the three possibilities: increased, unchanged, or decreased. Measurements of rate-level slopes using a preparation similar to that of Miller *et al.* are consistent with this expectation (M. G. Heinz, personal communication). Thus Geisler's argument, while correct, does not apply to mixed losses of the type considered here.

Our method of separately determining OHC and IHC damage (see Secs. III B and III C) is consistent with the conclusion that both were present in the impaired cats of Miller *et al.* (1997), although histological analysis was not performed on these cochleae. Furthermore, the extent (i.e., BF region) of IHC impairment [Fig. 6(a)] is greater than the extent of OHC impairment [Fig. 5(a)], in agreement with the histological data described previously (Liberman, 1984; Liberman and Dodds, 1984a, b). IHC impairment was achieved in the model by decreasing the slope of the IHC nonlinearity. However, it is not clear what could be the physiological correlate of this manipulation. Permanently closed transduction channels (e.g., Pickels *et al.*, 1987) could lead to a reduced saturation potential and reduced maximum AN discharge rate, not seen in the data (Miller *et al.*, 1997). Permanently open transduction channels (Meyer *et al.*, 1998) would likely result in a large increase in the resting IHC potential and perhaps also in the spontaneous discharge rate of AN fibers, also not seen in the physiological data (Liberman and Dodds, 1984b; Miller *et al.*, 1997). More consistent with the AN data would be disarray of the stereociliar bundle (Liberman and Dodds, 1984a), such that greater pressure is required to reach both threshold and IHC saturation.

C. Future model improvements

The results of this study show good qualitative prediction of the effects of acoustic trauma on synchrony to a vowel, but the quantitative accuracy could benefit from improvements to the model. One possibility is that our methods of creating OHC and IHC impairment are too simple to capture the complex biophysical consequences of the mechanical trauma and subsequent cellular damage. A second possibility is that the inaccuracy of the *normal* model at high presentation levels, as seen in Sec. IV B, may produce similar inaccuracies in predicting the impaired data. Two physiological phenomena that are not included in the normal model and which may help explain its inaccuracy at high presentation levels are frequency glides and multi-modal excitation.

Frequency glides are modulations or sweeps in the instantaneous frequency of the impulse response of BM filters, also reflected in the impulse response of AN fibers (Carney *et al.*, 1999). Carney *et al.* (1999) found that the impulse response has an upward frequency glide for fibers with BFs greater than 1500 Hz, almost no glide for BFs between 750 and 1500 Hz, and a downward glide for BFs less than 750 Hz. They also found that glides are independent of stimulus intensity, but pointed out that the interaction of the glide with the nonlinear envelope of the impulse response could lead to shifts in BF with level. Broad filters have short time constants and, consequently, their response will be dominated

more by the starting frequency of the glide; narrow filters have long time constants and will therefore be dominated more by the final frequency of the glide. This level-dependent behavior may at least partially explain the BF shifts in BM tuning observed in the impaired cochlea and at high intensities in the normal cochlea (e.g., Robles and Ruggero, 2001). The lack of a BF shift may contribute to the model's inaccuracy in predicting the Wong *et al.* (1998) data (see Fig. 13); a larger downward BF shift at high intensities could reduce synchrony to $F2$ and increase synchrony to $F1$. This is consistent with the growth of low-side two-tone rate suppression in the model, which is also weaker than is observed in physiological data (Zhang *et al.*, 2001).

Multi-modal excitation is the presence of more than one vibrational mode in the BM response because of the complex micromechanics of the organ of Corti (e.g., Robles and Ruggero, 2001). Such multi-modal excitation, also observed in AN responses (Lin and Guinan, 2000), cannot be explained by a single-path BM filter as used in our model; parallel paths are required to model each mode of vibration (Goldstein, 1990; Schoonhoven *et al.*, 1994; Meddis *et al.*, 2001). In multi-path models, the center frequencies of each of the parallel filters are typically different, which along with the frequency glide in individual filters could contribute to shifts in BF with OHC impairment or at high presentation levels (Goldstein, 1990; Schoonhoven *et al.*, 1994; Meddis *et al.*, 2001). The interactions of the different paths might also explain the C1/C2 transition (Lieberman and Kiang, 1984; Wong *et al.*, 1998).

One feature not considered in any of these models is the stapedial reflex, which has been shown to reduce the upward spread of masking (i.e., low-side suppression) in AN fibers (Pang and Guinan, 1997). The physiological data examined in this paper (Miller *et al.*, 1997; Wong *et al.*, 1998; Miller *et al.*, 1999a) were from anesthetized cats in which the reflex is not present, and therefore modeling of the reflex is not necessary to describe the data. However, if the data and modeling results are to be applicable to hearing-aid design, then the stapedial reflex could be a significant factor in determining the AN response to vowels in hearing-impaired individuals. The ME section of our model could be adapted to describe the effects of the stapedial reflex. This would create another time-varying, nonlinear filter, and the control signal for the reflex could likely be obtained from a large population of model fibers.

Additionally, it is known that fibers with different spontaneous rates (and corresponding thresholds) provide different representations of speech stimuli across stimulus intensities (Sachs and Young, 1979). In particular, low and medium spontaneous rate fibers provide a better representation of vowels in their average discharge rates at high intensities. It would therefore be useful to extend the synapse model to be able to produce an arbitrary spontaneous rate and the associated change in the rate-level function (Sachs and Abbas, 1974; Yates, 1990).

The major deviation between the model and data is the difference in response to $F2$ in the impaired case (Fig. 16). This difference is apparently related to the weak suppression of $F2$ by $F1$ shown in Fig. 13. While the main cause is

probably the fact that the Zhang *et al.* (2001) model produces insufficient two-tone suppression for suppressors below BF, other factors may contribute. We have already argued that the lack of frequency glides in the model's filters could contribute to this difference. Another possibility, related to the modeling of low and medium spontaneous rate (higher threshold) fibers, is the fact that the model incorporates only the minimal threshold shift [Fig. 6(b)]. Additional threshold shift to model the average thresholds in the data would require a decrease in the IHC/synapse gain. As discussed above, decreases in IHC synapse gain have the effect of reducing large-signal suppression in the IHC and synapse and result in more broadband responses. Thus if the full range of thresholds were modeled, then the model data in Fig. 16 would scatter in the direction of lower synchrony to $F2$, which would decrease the difference between model and data.

D. Applicability of the model to hearing-aid design

The model presented in this paper appears accurate enough to be useful in testing the effects of potential hearing-aid processing schemes on the neural representation of speech. Such testing would provide information about hearing aids to supplement that provided by psychophysics and perceptual testing. Because the primary lesion in hearing impairment is usually in the cochlea, it seems clear that a useful goal for hearing-aid design should be producing auditory nerve responses that are as normal as possible. The value of the model in this regard is that it is much simpler, more flexible, and cheaper than physiological experiments. As a validation of the model's usefulness in this regard, it predicts both the benefits and the limitations of the CEFS amplification scheme (Sec. IV D), as they were observed in physiological experiments. There are two limitations on the usefulness of the model for such testing: first, there is the uncertainty about the quantitative relationship of cat and human auditory nerve responses. Recio *et al.* (2002) have argued that suppressive interactions among the formants and upward spread of $F1$ may be a smaller issue in the human cochlea, because of its longer length relative to the range of frequencies represented. Thus the model will have to be modified and validated for the human auditory periphery (Heinz *et al.*, 2001). Second, there is no direct way, at present, of estimating the specific degree of IHC and OHC impairment in individual human subjects. Methods of diagnosing IHC and OHC impairment are beginning to be developed (Moore *et al.*, 1999, 2000; Plack and Oxenham, 2000), but these methods do not yet provide a practical method of diagnosing individuals' degrees of hair cell damage. Nevertheless, the model can still provide valuable information by evaluating the effectiveness of signal processing for various commonly encountered lesions.

ACKNOWLEDGMENTS

The authors would like to thank Xuedong (Frank) Zhang, Michael Heinz, and Laurel Carney for providing source code for the Zhang *et al.* (2001) auditory-periphery model and for discussions on improving the normal model;

Bill Peake for invaluable assistance with the middle-ear model; Roger Miller for supplying physiological data; and Brad May, Kevin Davis, Michael Heinz, Laurel Carney, Ray Meddis, and three anonymous reviewers for helpful comments on earlier versions of the manuscript. This research was supported by NIDCD Grant Nos. DC00109 and DC00023.

APPENDIX A: MIDDLE-EAR MODEL

The ME section of the auditory-periphery model was created by combining the ME cavities model of Peake *et al.* (1992) with the ME model of Matthews (1983). Both of these are based on data from cats and are therefore suitable for use in this model. An electrical-circuit representation of the composite model is shown in Fig. 19(a); circuit-element values are given in Table II. The circuit was simplified by omitting the round-window compliance C_{rw} , which does not produce any significant change in the transfer function.

A transfer-function representation $G(s)$ of the circuit (i.e., the transfer of pressure outside the eardrum to pressure across the cochlear partition) was determined using the computer program SAPWIN (Liberatore *et al.*, 1995), giving

$$G(s) = \frac{\text{NUM}(s)}{\text{DEN}(s)}, \quad (\text{A1})$$

where

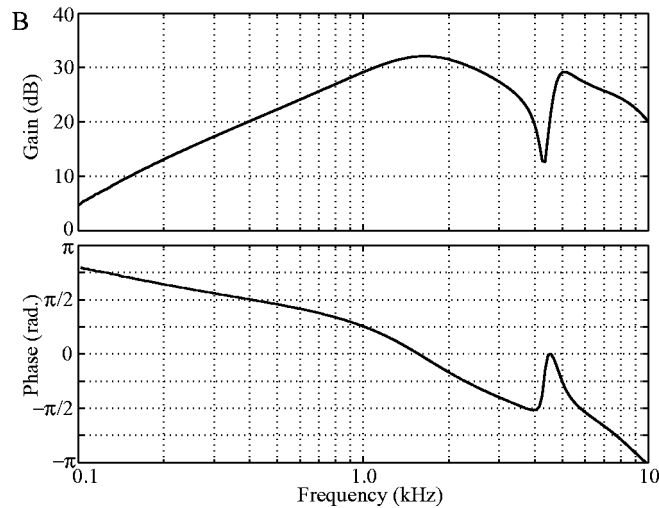
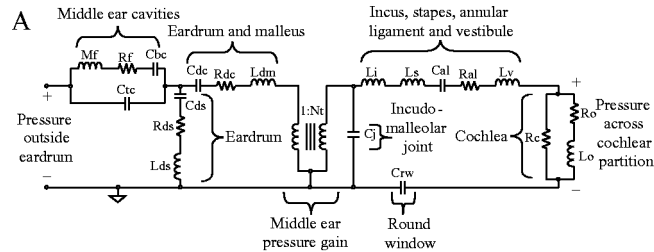


FIG. 19. (a) Electrical-circuit representation of middle-ear model. Circuit-element values are given in Table II. (b) Gain (top panel) and phase (bottom panel) of the frequency response of the middle-ear model shown in (a).

TABLE II. Circuit-element values for the middle-ear model. Values for M_f , R_f , C_{bc} , and C_{tc} are taken from the caption of Fig. 4 in Peake *et al.* (1992) and converted into cgs-units for compatibility with the units used by Matthews (1983) for all the other values: [pressure] = dyne/cm² = [voltage] = volt; [volume velocity] = cm³/s = [current] = ampere; [acoustic compliance] = cm⁵/dyne = [capacitance] = farad; [acoustic mass] = g/cm⁴ = [inductance] = henry; [acoustic damping] = dyne · s/cm⁵ = [resistance] = ohm; [acoustic impedance] = dyne · s/cm⁵ = [impedance] = ohm.

$M_f = 0.0101$	$C_j = 1.2 \times 10^{-11}$
$R_f = 13.7$	$L_i = 1.6$
$C_{bc} = 5.55 \times 10^{-7}$	$L_s = 3.3$
$C_{tc} = 1.75 \times 10^{-7}$	$L_v = 22$
$C_{ds} = 8 \times 10^{-8}$	$C_{al} = 3.7 \times 10^{-10}$
$R_{ds} = 1300$	$R_{al} = 2 \times 10^5$
$L_{ds} = 0.054$	$R_c = 1.2 \times 10^6$
$C_{dc} = 3.5 \times 10^{-7}$	$R_o = 2.8 \times 10^5$
$R_{dc} = 55.2$	$L_o = 2250$
$L_{dm} = 0.04$	$C_{rw} = 1 \times 10^{-8}$
$N_t = 55$	

$$\begin{aligned} \text{NUM}(s) = & 4.07874 \times 10^{-55} s^8 + 1.04232 \times 10^{-50} s^7 \\ & + 4.1255 \times 10^{-46} s^6 + 7.48636 \times 10^{-42} s^5 \\ & + 7.1186 \times 10^{-38} s^4 + 8.74363 \times 10^{-36} s^3, \end{aligned} \quad (\text{A2})$$

and

$$\begin{aligned} \text{DEN}(s) = & 2.41138 \times 10^{-70} s^{11} + 1.91739 \times 10^{-65} s^{10} \\ & + 1.60971 \times 10^{-60} s^9 + 5.76989 \times 10^{-56} s^8 \\ & + 1.90447 \times 10^{-51} s^7 + 3.87288 \times 10^{-47} s^6 \\ & + 5.37782 \times 10^{-43} s^5 + 4.18754 \times 10^{-39} s^4 \\ & + 1.99923 \times 10^{-35} s^3 + 1.20211 \times 10^{-32} s^2 \\ & + 2.61157 \times 10^{-44} s, \end{aligned} \quad (\text{A3})$$

and s is in units of rad/s. From this continuous-time transfer function, a tenth-order, IIR digital filter was created using the `invfreqz` function in MATLAB (The MathWorks, Natick, MA) with a sampling frequency of 100 kHz.² The gain and phase of the frequency response of the digital filter are shown in Fig. 19(b).

APPENDIX B: IMPROVED DYNAMICS FOR OHC CONTROL OF THE BM FILTER

The dynamics of BM compression and suppression (Robles *et al.*, 1976; Ruggero and Rich, 1991) are determined in the model by the combination of the control-path OHC nonlinearity (a Boltzmann function) and the OHC LP filter [see Fig. 1(a)]. The wideband filter of Zhang *et al.* (2001) has a varying bandwidth, but the gain at BF is normalized to unity at each time step. With the prescribed asymmetry for the Boltzmann function, the control path produces compression in the signal path only over a restricted dynamic range (<30 dB), so Zhang *et al.* added a symmetrical, compressive nonlinearity between the wideband filter and the Boltzmann function to extend this dynamic range (see Fig. 1 of Zhang *et al.*, 2001). However, we have found that this

nonlinearity introduces distortion products into τ_{sp} and τ_{cp} for multi-tone or vowel stimuli, which induce the same undesired distortion products into the output of the signal-path, narrow-band filter. These distortion products can be avoided if compression in the control path is produced not by a static nonlinearity but rather by dynamic compression in the wide-band filter, as it is for the narrow-band filter. This is achieved by normalizing the gain at BF not to unity but rather to the gain of the narrow-band (signal path) filter, such that both filters have roughly the same output for a BF tone.³

The gain normalization is achieved by first setting the gain of each control-path low-pass filter to unity at BF. The filter coefficients are calculated for the present value of $\tau_{cp}[n]$ {using Eqs. (3) and (4) with $\tau_{cp}[n]=K\tau_{sp}[n]$ instead of $\tau_{sp}[n]$ }. The center frequency of the control-path wide band filter is not at BF but rather shifted to a frequency corresponding to a point on the basilar membrane 1.2 mm basal to the fiber BF, i.e., higher in frequency than BF (Zhang *et al.*, 2001). Consequently, the gain ($gain_{cp}[n]$) and the group delay ($grd_{cp}[n]$) at BF can be calculated for the control-path filter according to the equations [see pp. 213–230 of Oppenheim and Schaffer (1989)]:

$$gain_{cp}[n] = \sqrt{\frac{1 + c1_{LP}[n]^2 - 2c1_{LP}[n]\cos((\omega_{cp} - \omega_{BF})/F_s)}{2c2_{LP}[n]^2(1 - \cos((\omega_{cp} - \omega_{BF})/F_s))}} \quad (B1)$$

and

$$grd_{cp}[n] = 0.5 - \frac{c1_{LP}[n]^2 - c1_{LP}[n]\cos((\omega_{cp} - \omega_{BF})/F_s)}{1 + c1_{LP}[n]^2 - 2c1_{LP}[n]\cos((\omega_{cp} - \omega_{BF})/F_s)}, \quad (B2)$$

where ω_{BF} is the radian frequency ($2\pi \times BF$) corresponding to the fiber's BF and ω_{cp} is the center radian frequency of the wideband filter. The gain normalization is applied to the filter by multiplying $c2_{LP}[n]$ by $gain_{cp}[n]$ as given by Eq. (B1) after the number of samples given by the group delay has elapsed. That is, the gain normalization value is delayed to match the group delay. The gain might not be set for every sample because of the fluctuating group delay, in which case the most recent value for the gain normalization is used. After the gain at BF for each of the low-pass filters has been set to unity, the output of the entire wideband filter is multiplied by $(\tau_{sp}[n]/\tau_{narrow})^3$ to make its gain track that of the narrow-band filter.

This method of normalizing the gain does not correct for the phase changes with $\tau_{cp}[n]$. The phase changes could be compensated for by a time-varying all-pass filter, but we have not found this necessary in our simulations if we (i) reduce the cutoff frequency of the LP filter following the OHC nonlinearity [see Fig. 1(a)] from 800 to 600 Hz and (ii) ensure that the magnitude of the cochlear-amplifier gain for BFs less than 3 kHz is not too large.

Note that in our version of the model, the output of the wideband filter is also multiplied by a scaling factor of 4×10^3 at the input to the Boltzmann function to compensate

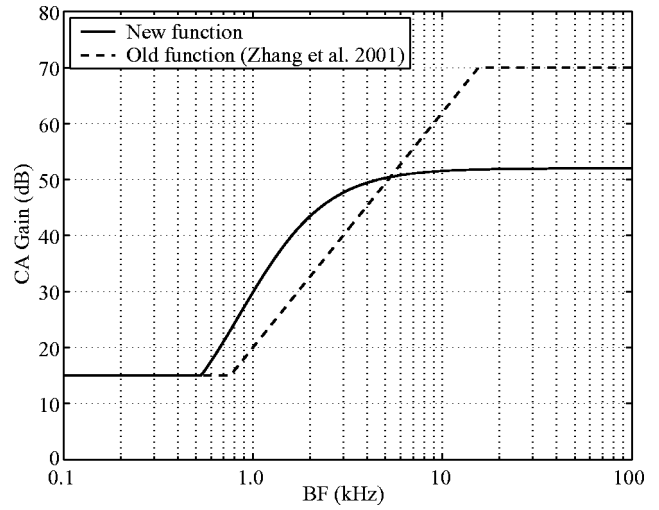


FIG. 20. Cochlear amplifier gain versus BF. The dashed line shows the function used in Zhang *et al.* (2001), and the solid line shows the new function described by Eq. (B3).

for the removal of the symmetrical nonlinearity, that is, so that the published parameters for the Boltzmann function are still appropriate.

We have also found it necessary to modify how much CA gain [see Fig. 4(b)] is applied at each BF to explain (i) the change in Q_{10} values for impaired AN fibers (see Sec. III B) and (ii) AN vowel responses at high stimulus intensities (see Sec. IV B). Equation (7) of Zhang *et al.* (2001) has been modified to

$$gain_{CA}(BF) = \max\{15, 52(\tanh(2.2 \log_{10}(BF) + 0.15) + 1)/2\}, \quad (B3)$$

where BF is in the units of kHz. Plotted in Fig. 20 are the old (dashed line) and new (solid line) functions for CA gain. The old function was quite arbitrary and was roughly based on BM data from guinea pigs and chinchillas; such BM data do not exist for cats. While the new function is still arbitrary and was obtained indirectly by looking at the degradation of tuning in impaired fibers and at responses to vowel stimuli, it may provide a more accurate estimate of cochlear amplifier gain for cats. One indication of this is that the maximum gain is now 52 dB instead of 70 dB: high-BF, low-spontaneous-rate model fibers with 70 dB of gain have “straight” rate-level functions (Heinz *et al.*, 2001) which are observed in guinea pigs and chinchillas but not in cats (Sachs and Abbas, 1974); reducing the gain to 52 dB for high-BF fibers produces “sloping-saturation” rate-level functions, as observed in cats (results not shown).

³Scaling τ_{sp} in this fashion produces a linear change in the filter's Q_{10} as a function of C_{OHC} . For example, if $C_{OHC}=0.5$, then the filter's Q_{10} will be halfway between the filter's Q_{10} value for normal OHC function ($C_{OHC}=1$) and its Q_{10} value for complete OHC impairment ($C_{OHC}=0$). We have chosen this method of scaling τ_{sp} because in Sec. III B we use Q_{10} values from physiological data to set the level of OHC impairment as a function of BF. The filter gain at BF is $(\tau_{sp_impaired}[n]/\tau_{narrow})^3$, and consequently the impaired gain (either linear or in dB) does not change linearly with C_{OHC} [see Fig. 1(b)]. It is possible to apply an alternative scaling method

$$\tau_{sp_impaired}[n] = \tau_{sp}[n](\tau_{wide}/\tau_{sp}[n])^{1-C'_{OHC}},$$

so that the gain in dB changes linearly with an alternative scaling factor C'_{OHC} .

²This sampling frequency is sufficient to produce an accurate and stable filter over the important frequency range (0.1–10 kHz). Even so, care must be taken to ensure stability when implementing the filter with fixed-precision algorithms—please contact the authors for further advice on this issue.

³The outputs of the narrow- and wideband filters will not be identical for a BF tone because (i) the center-frequency of the wideband filter is above BF and consequently the phase at BF fluctuates with $\tau_{\text{cp}}[n]$ and (ii) the wideband filter, in contrast to the narrow-band filter, is not followed by a linear band-pass filter.

Anderson, D. J., Rose, J. E., Hind, J. E., and Brugge, J. F. (1971). “Temporal position of discharges in single auditory nerve fibers within the cycle of a sine-wave stimulus: Frequency and intensity effects,” *J. Acoust. Soc. Am.* **49**, 1131–1139.

Bruce, I. C., Young, E. D., and Sachs, M. B. (1999). “Modification of an auditory-periphery model to describe the effects of acoustic trauma on auditory nerve response,” in *Abstracts of the 22nd ARO Midwinter Meeting*.

Carney, L. H. (1993). “A model for the responses of low-frequency auditory-nerve fibers in cat,” *J. Acoust. Soc. Am.* **93**, 401–417.

Carney, L. H., McDuffy, M. J., and Shekhter, I. (1999). “Frequency glides in the impulse responses of auditory-nerve fibers,” *J. Acoust. Soc. Am.* **105**, 2384–2391.

Costalupes, J. A., Rich, N. C., and Ruggero, M. A. (1987). “Effects of excitatory and non-excitatory suppressor tones on two-tone rate suppression in auditory nerve fibers,” *Hear. Res.* **26**, 155–164.

Delgutte, B. (1990). “Two-tone rate suppression in auditory-nerve fibers: Dependence on suppressor frequency and level,” *Hear. Res.* **49**, 225–246.

Deng, L., and Geisler, C. D. (1987a). “A composite auditory model for processing speech sounds,” *J. Acoust. Soc. Am.* **82**, 2001–2012.

Deng, L., and Geisler, C. D. (1987b). “Responses of auditory-nerve fibers to nasal consonant-vowel syllables,” *J. Acoust. Soc. Am.* **82**, 1977–1988.

Deng, L., Geisler, C. D., and Greenberg, S. (1987). “Responses of auditory-nerve fibers to multiple-tone complexes,” *J. Acoust. Soc. Am.* **82**, 1989–2000.

Duifhuis, H. (1976). “Cochlear nonlinearity and second filter: Possible mechanism and implications,” *J. Acoust. Soc. Am.* **59**, 408–423.

Gao, W. Y., Ding, D. L., Zheng, X. Y., Ruan, F. M., and Liu, Y. J. (1992). “A comparison of changes in the stereocilia between temporary and permanent hearing losses in acoustic trauma,” *Hear. Res.* **62**, 27–41.

Geisler, C. D. (1981). “A model for discharge patterns of primary auditory-nerve fibers,” *Brain Res.* **212**, 198–201.

Geisler, C. D. (1985). “Effects of a compressive nonlinearity in a cochlear model,” *J. Acoust. Soc. Am.* **78**, 257–260.

Geisler, C. D. (1989). “The responses of models of ‘high-spontaneous’ auditory-nerve fibers in a damaged cochlea to speech syllables in noise,” *J. Acoust. Soc. Am.* **86**, 2192–2205.

Giguère, C., and Woodland, P. C. (1994). “A computational model of the auditory periphery for speech and hearing research. II. Descending paths,” *J. Acoust. Soc. Am.* **95**, 343–349.

Goldstein, J. L. (1990). “Modeling rapid waveform compression on the basilar membrane as multiple-bandpass-nonlinearity filtering,” *Hear. Res.* **49**, 39–60.

Goldstein, J. L. (1995). “Relations among compression, suppression, and combination tones in mechanical responses of the basilar membrane: Data and MBPNL model,” *Hear. Res.* **89**, 52–68.

Guinan, Jr., J. J., and Peake, W. T. (1967). “Middle-ear characteristics of anesthetized cats,” *J. Acoust. Soc. Am.* **41**, 1237–1261.

Harrison, R. V. (1981). “Rate-versus-intensity functions and related AP responses in normal and pathological guinea pig and human cochleas,” *J. Acoust. Soc. Am.* **70**, 1036–1044.

Heinz, M. G., Zhang, X., Bruce, I. C., and Carney, L. H. (2001). “Auditory nerve model for predicting performance limits of normal and impaired listeners,” *ARLO* **2**, 91–96.

Irino, T., and Patterson, R. D. (2001). “A compressive gammachirp auditory filter for both physiological and psychophysical data,” *J. Acoust. Soc. Am.* **109**, 2008–2022.

Javel, E., Geisler, C. D., and Ravindran, A. (1978). “Two-tone suppression in auditory nerve of the cat: Rate-intensity and temporal analyses,” *J. Acoust. Soc. Am.* **63**, 1093–1104.

Javel, E., McGee, J., Walsh, E. J., Farley, G. R., and Gorga, M. P. (1983).

“Suppression of auditory nerve responses. II. Suppression threshold and growth, iso-suppression contours,” *J. Acoust. Soc. Am.* **74**, 801–813.

Jenison, R. L., Greenberg, S., Kluender, K. R., and Rhode, W. S. (1991). “A composite model of the auditory periphery for the processing of speech based on the filter response functions of single auditory-nerve fibers,” *J. Acoust. Soc. Am.* **89**, 773–786.

Johnstone, B. M., Patuzzi, R., and Yates, G. K. (1986). “Basilar membrane measurements and the travelling wave,” *Hear. Res.* **22**, 147–153.

Kates, J. M. (1995). “Two-tone suppression in a cochlear model,” *IEEE Trans. Speech Audio Process.* **3**, 396–406.

Kiang, N. Y., Liberman, M. C., and Levine, R. A. (1976). “Auditory-nerve activity in cats exposed to ototoxic drugs and high-intensity sounds,” *Ann. Otol. Rhinol. Laryngol.* **85**, 752–768.

Liberatore, A., Luchetta, A., Manetti, S., and Piccirilli, M. C. (1995). “A new symbolic program package for the interactive design of analog circuits,” in *ISCAS’95, IEEE International Symposium on Circuits and Systems, 1995, Vol. 3* (IEEE, Piscataway, NJ), pp. 2209–2212.

Liberman, M. C. (1978). “Auditory nerve response from cats raised in a low noise chamber,” *J. Acoust. Soc. Am.* **63**, 442–455.

Liberman, M. C. (1984). “Single-neuron labeling and chronic cochlear pathology. I. Threshold shift and characteristic-frequency shift,” *Hear. Res.* **16**, 33–41.

Liberman, M. C., and Dodds, L. W. (1984a). “Single-neuron labeling and chronic cochlear pathology. III. Stereocilia damage and alterations of threshold tuning curves,” *Hear. Res.* **16**, 55–74.

Liberman, M. C., and Dodds, L. W. (1984b). “Single-neuron labeling and chronic cochlear pathology. II. Stereocilia damage and alterations of spontaneous discharge rates,” *Hear. Res.* **16**, 43–53.

Liberman, M. C., and Kiang, N. Y.-S. (1984). “Single-neuron labeling and chronic cochlear pathology. IV. Stereocilia damage and alterations in rate- and phase-level functions,” *Hear. Res.* **16**, 75–90.

Liberman, M. C., and Mulroy, M. J. (1982). “Acute and chronic effects of acoustic trauma: Cochlear pathology and auditory nerve pathophysiology,” in *New Perspectives on Noise-Induced Hearing Loss*, edited by R. P. Hamernik, D. Henderson, and R. Salvi (Raven, New York), pp. 105–135.

Lin, T., and Guinan, Jr., J. J. (2000). “Auditory-nerve-fiber responses to high-level clicks: Interference patterns indicate that excitation is due to the combination of multiple drives,” *J. Acoust. Soc. Am.* **107**, 2615–2630.

Lopez-Poveda, E. A., and Meddis, R. (2001). “A human nonlinear cochlear filterbank,” *J. Acoust. Soc. Am.* **110**, 3107–3118.

Lybarger, S. F. (1978). “Selective amplification—a review and evaluation,” *J. Am. Audiol. Soc.* **3**, 258–266.

Matthews, J. W. (1983). “Modeling reverse middle ear transmission of acoustic distortion signals,” in *Mechanics of Hearing: Proceedings of the IUTAM/ICA Symposium*, edited by E. de Boer and M. A. Viergever (Delft U. P., Delft), pp. 11–18.

Meddis, R., O’Mard, L. P., and Lopez-Poveda, E. A. (2001). “A computational algorithm for computing nonlinear auditory frequency selectivity,” *J. Acoust. Soc. Am.* **109**, 2852–2861.

Meyer, J., Furness, D. N., Zenner, H.-P., Hackney, C. M., and Gummer, A. W. (1998). “Evidence for opening of hair-cell transducer channels after tip-link loss,” *J. Neurosci.* **18**, 6748–6756.

Miller, R. L., Calhoun, B. M., and Young, E. D. (1999a). “Contrast enhancement improves the representation of /ε/-like vowels in the hearing-impaired auditory nerve,” *J. Acoust. Soc. Am.* **106**, 2693–2708.

Miller, R. L., Calhoun, B. M., and Young, E. D. (1999b). “Discriminability of vowel representations in cat auditory-nerve fibers after acoustic trauma,” *J. Acoust. Soc. Am.* **105**, 311–325.

Miller, R. L., Schilling, J. R., Franck, K. R., and Young, E. D. (1997). “Effects of acoustic trauma on the representation of the vowel /ε/ in cat auditory nerve fibers,” *J. Acoust. Soc. Am.* **101**, 3602–3616.

Moore, B. C., Glasberg, B. R., and Vickers, D. A. (1999). “Further evaluation of a model of loudness perception applied to cochlear hearing loss,” *J. Acoust. Soc. Am.* **106**, 898–907.

Moore, B. C., Huss, M., Vickers, D. A., Glasberg, B. R., and Alcantara, J. I. (2000). “A test for the diagnosis of dead regions in the cochlea,” *Br. J. Audiol.* **34**, 205–224.

Nordmann, A. S., Bohne, B. A., and Harding, G. W. (2000). “Histopathological differences between temporary and permanent threshold shift,” *Hear. Res.* **139**, 13–30.

Oppenheim, A. V., and Schaffer, R. W. (1989). *Discrete-Time Signal Processing* (Prentice-Hall, Englewood Cliffs, NJ).

Oxenham, A. J., and Plack, C. J. (1997). “A behavioral measure of basilar-

- membrane nonlinearity in listeners with normal and impaired hearing," *J. Acoust. Soc. Am.* **101**, 3666–3675.
- Pang, X. D., and Guinan, Jr., J. J. (1997). "Effects of stapedius-muscle contractions on the masking of auditory-nerve responses," *J. Acoust. Soc. Am.* **102**, 3576–3586.
- Patterson, R., Nimmo-Smith, I., Holdsworth, J., and Rice, P. (1988). "Implementing a gammatone filter bank," SVOS Final Report: The Auditory Filter Bank.
- Payton, K. L. (1988). "Vowel processing by a model of the auditory periphery: A comparison to eighth-nerve responses," *J. Acoust. Soc. Am.* **83**, 145–162.
- Peake, W. T., Rosowski, J. J., and Lynch, III, T. J. (1992). "Middle-ear transmission: Acoustic versus ossicular coupling in cat and human," *Hear. Res.* **57**, 245–268.
- Pfeiffer, R. R. (1970). "A model for two-tone inhibition of single cochlear-nerve fibers," *J. Acoust. Soc. Am.* **48**, 1373–1378.
- Pickles, J. O., Osborne, M. P., and Comis, S. D. (1987). "Vulnerability of tip links between stereocilia to acoustic trauma in the guinea pig," *Hear. Res.* **25**, 173–183.
- Plack, C. J., and Oxenham, A. J. (2000). "Basilar-membrane nonlinearity estimated by pulsation threshold," *J. Acoust. Soc. Am.* **107**, 501–507.
- Rocio, A., Rhode, W. S., Kieft, M., and Kluender, K. R. (2002). "Responses to cochlear normalized speech stimuli in the auditory nerve of cat," *J. Acoust. Soc. Am.* **111**, 2213–2218.
- Robert, A., and Eriksson, J. L. (1999). "A composite model of the auditory periphery for simulating responses to complex sounds," *J. Acoust. Soc. Am.* **106**, 1852–1864.
- Robertson, D. (1982). "Effects of acoustic trauma on stereocilia structure and spiral ganglion cell tuning properties in the guinea pig cochlea," *Hear. Res.* **7**, 55–74.
- Robles, L., and Ruggero, M. A. (2001). "Mechanics of the mammalian cochlea," *Physiol. Rev.* **81**, 1305–1352.
- Robles, L., Rhode, W. S., and Geisler, C. D. (1976). "Transient response of the basilar membrane measured in squirrel monkeys using the Mossbauer effect," *J. Acoust. Soc. Am.* **59**, 926–939.
- Ruggero, M. A., and Rich, N. C. (1991). "Application of a commercially-manufactured Doppler-shift laser velocimeter to the measurement of basilar-membrane vibration," *Hear. Res.* **51**, 215–230.
- Sachs, M. B., and Abbas, P. J. (1974). "Rate versus level functions for auditory-nerve fibers in cats: Tone-burst stimuli," *J. Acoust. Soc. Am.* **56**, 1835–1847.
- Sachs, M. B., and Kiang, N. Y. (1968). "Two-tone inhibition in auditory-nerve fibers," *J. Acoust. Soc. Am.* **43**, 1120–1128.
- Sachs, M. B., and Young, E. D. (1979). "Encoding of steady-state vowels in the auditory nerve: Representation in terms of discharge rate," *J. Acoust. Soc. Am.* **66**, 470–479.
- Sachs, M. B., Bruce, I. C., Miller, R. L., and Young, E. D. (2002). "Biological basis of hearing-aid design," *Ann. Biomed. Eng.* **30**, 157–168.
- Salvi, R., Henderson, D., and Hamernik, R. (1983). "Physiological bases of sensorineural hearing loss," in *Hearing Research and Theory*, edited by J. V. Tobias and E. D. Schubert (Academic, New York), pp. 173–231.
- Salvi, R., Perry, J., Hamernik, R. P., and Henderson, D. (1982). "Relationships between cochlear pathologies and auditory nerve and behavioral responses following acoustic trauma," in *New Perspectives on Noise-Induced Hearing Loss*, edited by R. P. Hamernik, D. Henderson, and R. Salvi (Raven, New York), pp. 165–188.
- Schilling, J. R., Miller, R. L., Sachs, M. B., and Young, E. D. (1998). "Frequency-shaped amplification changes the neural representation of speech with noise-induced hearing loss," *Hear. Res.* **117**, 57–70.
- Schmiedt, R. A., Mills, J. H., and Adams, J. C. (1990). "Tuning and suppression in auditory nerve fibers of aged gerbils raised in quiet or noise," *Hear. Res.* **45**, 221–236.
- Schmiedt, R. A., Zwillocki, J. J., and Hamernik, R. P. (1980). "Effects of hair cell lesions on responses of cochlear nerve fibers. I. Lesions, tuning curves, two-tone inhibition, and responses to trapezoidal-wave patterns," *J. Neurophysiol.* **43**, 1367–1389.
- Schoonhoven, R., Keijzer, J., Versnel, H., and Prijs, V. F. (1994). "A dual filter model describing single-fiber responses to clicks in the normal and noise-damaged cochlea," *J. Acoust. Soc. Am.* **95**, 2104–2121.
- Schroeder, M. R., and Hall, J. L. (1974). "Model for mechanical to neural transduction in the auditory receptor," *J. Acoust. Soc. Am.* **55**, 1055–1060.
- Temchin, A. N., Rich, N. C., and Ruggero, M. A. (1997). "Low-frequency suppression of auditory nerve responses to characteristic frequency tones," *Hear. Res.* **113**, 29–56.
- Wiener, F. M., and Ross, D. A. (1946). "The pressure distribution in the auditory canal in a progressive sound field," *J. Acoust. Soc. Am.* **18**, 401–408.
- Wong, J. C., Miller, R. L., Calhoun, B. M., Sachs, M. B., and Young, E. D. (1998). "Effects of high sound levels on responses to the vowel/eh/in cat auditory nerve," *Hear. Res.* **123**, 61–77.
- Yates, G. K. (1990). "Basilar membrane nonlinearity and its influence on auditory nerve rate-intensity functions," *Hear. Res.* **50**, 145–162.
- Young, E. D., and Sachs, M. B. (1979). "Representation of steady-state vowels in the temporal aspects of the discharge patterns of populations of auditory nerve fibers," *J. Acoust. Soc. Am.* **66**, 1381–1403.
- Zhang, M., and Zwillocki, J. J. (1996). "Intensity-dependent peak shift in cochlear transfer functions at the cellular level, its elimination by sound exposure, and its possible underlying mechanisms," *Hear. Res.* **96**, 46–58.
- Zhang, X., Heinz, M. G., Bruce, I. C., and Carney, L. H. (2001). "A phenomenological model for the responses of auditory-nerve fibers: I. Nonlinear tuning with compression and suppression," *J. Acoust. Soc. Am.* **109**, 648–670.